water

MDPI

Article

Evaluation of Past and Future Climate Trends under CMIP6 Scenarios for the UBNB (*Abay*), Ethiopia

Addis A. Alaminie [1,*], Seifu A. Tilahun [1], Solomon A. Legesse [2], Fasikaw A. Zimale [1], Gashaw Bimrew Tarkegn [2] and Mark R. Jury [3]

1 Faculty of Civil and Water Resources Engineering, Bahir Dar Institute of Technology, Bahir Dar University, Bahir Dar 6000, Ethiopia; satadm86@gmail.com (S.A.T.); fasikaw@gmail.com (F.A.Z.)
2 Department of NRM and Climate Change, College of Agriculture and Environmental Science, Bahir Dar University, Bahir Dar 6000, Ethiopia; soladd2000@yahoo.com (S.A.L.); gashbimrew@gmail.com (G.B.T.)
3 Physics Department, University of Puerto Rico Mayagüez, Mayagüez 00680, Puerto Rico; mark.jury@upr.edu
* Correspondence: metaddi@gmail.com; Tel.: +251-925-306-708

Abstract: Climate predictions using recent and high-resolution climate models are becoming important for effective decision-making and for designing appropriate climate change adaptation and mitigation strategies. Due to highly variable climate and data scarcity of the upper Blue Nile Basin, previous studies did not detect specific unified trends. This study discusses, the past and future climate projections under CMIP6-SSPs scenarios for the basin. For the models' validation and selection, reanalysis data were used after comparing with area-averaged ground observational data. Quantile mapping systematic bias correction and Mann–Kendall trend test were applied to evaluate the trends of selected CMIP6 models during the 21st century. Results revealed that, ERA5 for temperature and GPCC for precipitation have best agreement with the basin observational data, MRI-ESM2-0 for temperature and BCC-CSM-2MR for precipitation were selected based on their highest performance. The MRI-ESM2-0 mean annual maximum temperature for the near (long)-term period shows an increase of 1.1 (1.5) °C, 1.3 (2.2) °C, 1.2 (2.8) °C, and 1.5 (3.8) °C under the four SSPs. On the other hand, the BCC-CSM-2MR precipitation projections show slightly (statistically insignificant) increasing trend for the near (long)-term periods by 5.9 (6.1)%, 12.8 (13.7)%, 9.5 (9.1)%, and 17.1(17.7)% under four SSPs scenarios.

Keywords: Upper Blue Nile (*Abay*); temperature; precipitation; CMIP6; climate projection

Citation: Alaminie, A.A.; Tilahun, S.A.; Legesse, S.A.; Zimale, F.A.; Tarkegn, G.B.; Jury, M.R. Evaluation of Past and Future Climate Trends under CMIP6 Scenarios for the UBNB (*Abay*), Ethiopia. *Water* **2021**, *13*, 2110. https://doi.org/10.3390/w13152110

Academic Editor: Mavromatis Theodoros

Received: 14 June 2021
Accepted: 26 July 2021
Published: 31 July 2021

1. Introduction

Africa is the most vulnerable to climate change because of adverse direct effects on food security and national growth domestic product (GDP), and limited resilience to climate change [1,2]. The average percentage of poverty rates for East African countries is 38.83 and 38.08 in 2020 and 2021 respectively. In particular, East Africa, where the majority of the population are in poverty, is vulnerable to climate change and climate extremes [2,3]. The Intergovernmental Panel on Climate Change (IPCC's) fifth assessment report indicated that future climate change will lead to an increase in climate variability with the frequency and intensity of extreme events in the region [4].

One of the river basins in east Africa likely affected by climate change is the Upper Blue Nile Basin (UBNB). It drains a large area of the Ethiopian highlands and is the largest tributary of the Nile River, providing a vital source of freshwater to downstream riparian users in Sudan and Egypt. The effects of climate change on the future flow of the river and the effect to downstream countries is not well quantified [5,6].To quantify the impact of climate change on different sectors of the basin, research have been carried out using top-down approach of General/Global Circulation Models (GCMs) which have little local precision and has failed to address the regional consequences of climate change [7]. Previous studies [8–12] on the impacts of climate change in the Nile basin come up with highly

variable findings. Some of the plausible reasons are the higher variability of rainfall in the basin, insufficiency in temporal and spatial extent of analyzed data, different statistical measures used in each study [11,13]. GCMs cannot even agree on the signs; some have a positive sign (increase) and others have a negative sign (decrease) in the same region of study from different studies. Therefore, predicting future climates by studying past trends and using recent high-resolution climate models scenarios can be an effective method [5].

Data scarcity in the basin hampered understanding of the climate and hydrological processes that is required for sustainable water resource management. Reliable climate information is the basis for developing a climate-resilient system and intervention mechanisms to minimize the vulnerability of the region to various climatic risks [14]. Currently, Ethiopia is constructing the Great Ethiopian Renaissance Dam over the UBNB which requires research based adequate future climate effects of the dam and the basin [15–17].

As suggested in different guidelines and documentations developed by the IPCC, climate projections at relevant temporal and spatial scales are essential to assess potential future climate change impacts on climatologically diverse regions such as the UBNB [18,19]. The major challenge in climate change projections is the selection of an appropriate subset of GCMs. GCM simulations are associated with large uncertainties due to model resolution, mathematical formulation, initial assumptions, and calibration processes that restrict the use of all GCMs for reliable projections of climate at the regional or local scale [20,21]. Mostly it is assumed that more up-to-date, higher-resolution, and more complex models will perform better and produce more robust projections than previous-generation models [22].

The most recent state-of-the-art climate model experiments are now becoming available as part of the Coupled Model Intercomparison Project Phase 6 (CIMP6) ensemble. CMIP6 models are running a number of new and updated emission pathways that explore a much wider range of possible future outcomes than were included in CMIP5. CMIP6 represents a substantial expansion over CMIP5, in terms of the number of modelling groups participating, the number of future scenarios examined and the number of different experiments conducted.

The CMIP6 GCMs differ from previous generations, including high spatial resolutions, enhanced parameters of the cloud microphysical process, additional earth system processes and components such as biogeochemical cycles and ice sheets [23,24]. The major difference between CMIP5 and CMIP6 is the future scenarios CMIP5 projections are available on the basis of 2100 radiative forcing values for four GHG concentration pathways [25]. In contrast, CMIP6 uses socioeconomic pathways (SSPs) which are considered as more realistic future scenarios [26]. Another update of CMIP6 is the development and support of the intercomparison model, focusing on biases, processes, and climate model feedbacks [27]. The SSPs are based on five narratives describing alternative socio-economic developments, including sustainable development, regional rivalry, inequality, fossil-fueled development, and middle-of-the-road development. The objective of this research is therefore to evaluate and project the past and future climate trends using recent high-resolution climate models under different SSPs to overcome data scarcity issues. In order to select climate models for future projections, the model simulations of the historical climate have to be assessed and validated against reliable observational data with good spatial coverage to determine the skill and uncertainty of the models.

2. Materials and Methods

2.1. Study Area

Upper Blue Nile River (locally known as *Abay*) Basin is located in the northwestern part of Ethiopia between 7°45′ and 12°45′ N and 34°05′ and 39°45′ E and has a drainage area of about 176,652 km^2 [10,13]. The topography of the UBNB (UBNB) is composed of hills, highlands, valleys, and rock peaks. The most common land use feature of the basin is cultivated land with rainfed agriculture covering 64% of the basin. The Blue Nile River runs from its origin, Gish-Abbay, to the Sudanese border, and eventually meets the White Nile

River at Khartoum, Sudan. The length of the upper Blue Nile River from the outlet Lake Tana to the Ethio-Sudan border is 944.5 km [11]. Most of the streams feeding the Blue Nile are perennial [5]. The upper BNB contributes to around 70 percent (48.5 billion m^3 $year^{-1}$) of the total annual flow component of the main Nile [10,28].

The UBNB covers 17% of Ethiopia's surface area, generates 43% of the country's total average runoff, and is home to about 25% of its total population [29]. The UBNB's elevation ranges from 350m a.m.s.l near the Sudanese border to 4239 m a.m.s.l in the central part of the basin [30], for detail see Figure 1 below. The climate of the basin varies significantly according to the altitude and is governed by the seasonal migration of the Inter-Tropical Convergence Zone (ITCZ) [31]. The basin receives considerable amount of annual precipitation ranging between 800 and 2200 mm [10,32,33]. The mean annual temperature from 1961 to 1990 estimated to be 18.3 °C with a seasonal variation of less than 2 °C, and the annual potential evapotranspiration about 1100 mm [32]. The Blue Nile River discharge regime is highly seasonal with over 80% of its annual discharge occurring from July to October, and only 4% from January to April [34].

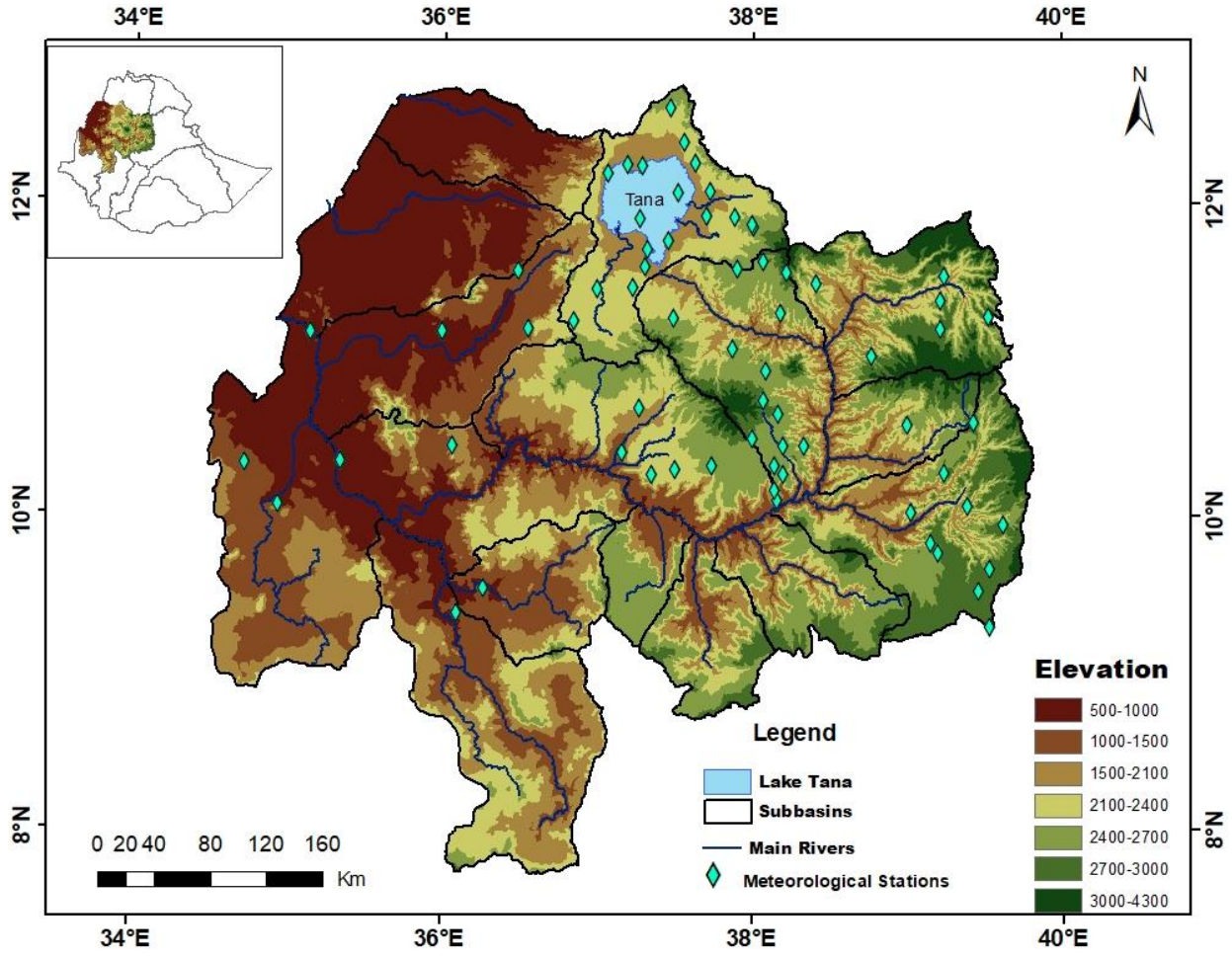

Figure 1. The geographical location of the Upper Blue Nile Basin (*Abay*) and meteorological station locations.

2.2. Data Set

Temperature and precipitation monthly observational, reanalysis, and CMIP6 model products over the UBNB (*Abay*) were retrieved from the Royal Netherlands Meteorological Institute (KNMI) Climate Explorer website and the World Climate Research Program (WCRP). Temperature and precipitation monthly observational data were extracted from the Climatic Research Unit (CRU TS 4.04) [35] and Global Precipitation Climatology Centre (GPCCv2020) [36]. Reanalysis products also derived from European Community Medium-

range Weather Forecasts v5 (ECMWF-ERA5) [37], NOAA-Climate Forecast System Reanalysis v2 (CFSR) [38] and NASA-MERRA v2 Modern Reanalysis [39]. For the future climate projection and trend analysis of the basin, data were extracted from the World Climate Research Programme's (WCRP)-CMIP6 under low forcing scenario (SSP1-2.6), a medium forcing scenario (SSP2-4.5), medium to high forcing scenario (SSP3-7.0), and a strong forcing scenario (SSP5-8.5). The detail description of scenarios is available in [22,24] and CMIP6 products are summarized in Table 1 which gives acronyms, resolution, sources, and references. For validation, available ground observation climatological data within the basin and for the baseline period (1981–2010) were collected from the archive of the National Meteorology Agency (NMA) of Ethiopia.

Table 1. List of employed CMIP6 climate models for evaluation and projection of the UBNB climate.

No.	CMIP6 Model Name	Country	Horizontal Res (lon. × lat. deg)	Key References
1.	BCC-CSM2-MR	China	1.1° × 1.1°	[40]
2.	CAMS-CSM1-0	China	1.1° × 1.1°	[40]
3.	CanESM5p1	Canada	2.8° × 2.8°	[41]
4.	CanESM5p2	Canada	2.8° × 2.8°	[41]
5.	CESM2	USA	1.3° × 0.9°	[42]
6.	CESM2-WACCM	USA	1.3° × 0.9°	[43]
7.	FGOALS-g3	China	2° × 2.3°	[44]
8.	MCM-UA-1-Of2	USA	2.5° × 2.5°	[45]
9.	MIROC6	Japan	1.4° × 1.4°	[46]
10.	MIROC-ES2L	Japan	2.8° × 2.8°	[46]
11.	MRI-ESM2-0	Japan	1.1° × 1.1°	[27]
12.	UKESM1-0-LL	UK	1.9° × 1.3°	[47]

2.3. Baseline Period Reanalysis and Monthly Observation Validation

The most important time series data necessary for this research is monthly precipitation and temperature data. Even though there are 202 meteorological stations in the basin, only 67 stations that have greater than 30 years were processed. For 21 stations, an attempt was made in estimating the missing data for those having less than 10% missing data for each station. These missed data have been estimated by using Markov chain simulation model of INSTAT [48]. This statistical package fits a model to the past data and then generates similar time series for any number of desired years. The monthly observational and reanalysis of temperature and precipitation data were validated with the ground observations using statistical measures such as the root mean square error (RMSE), coefficient of determination (R^2) and Nash–Sutcliffe Efficiency (NSE). These statistical measures determine different aspects of the data's accuracy for the purpose of CMIP6 model validation and selection for climate projections in the UBNB (area-average of 7°45′ & 12°45′ N and 34°05′ & 39°45′ E) over the period 1981–2010.

2.4. Climate Models Bias Correction

It is common that regional climate models (RCM) simulations are known to exhibit systematic biases in precipitation and temperature. In order to produce reliable estimators of local scale climate, RCM need to be post processed. Popular quantile mapping (QM) approaches implement statistical transformations for post-processing of climate modeling outputs. The statistical methods involve transforming the distribution functions of the modeled variables into the observed ones using a mathematical function. These transformations are mathematically expressed [49] as $x^o = f(x^m)$; in which x^o = observed variable; x^m = modeled variable; and f () = transformation function. The QM methods use the quantile-quantile relation to converge the simulated variables' distribution function to the observed one. The cumulative distribution functions (CDFs) of both observed and

simulated variable time series, their quantile relation can also be determined, as shown below [50]:

$$x^o = f_o{}^{-1}[F_m(x^m)]$$

where, $F_m(x^m)$ = CDF of x^m; and $f_o{}^{-1}$ = inverse form of the CDF of x^o, which is technically referred to as the quantile function. The quantile mapping attempts to adjust the distribution of modelled data such that it closely resembles the observed climatology. Practical evaluation of a wide range of QM methods showed that most of them are capable to remove biases in RCM precipitation especially non-parametric transformations have the highest skill in systematically reducing biases in RCM precipitation [51].

In this study, for precipitation and temperature bias correction, non-parametric QM methods were applied by checking their suitability using Nash-Sutcliff efficiency (NSE) and Mean Absolute Error (MAE) statistical measures of model climatology (1981–2010). Before evaluating precipitation and temperature for the dozen CMIP6 models, biases were corrected over the basin (*Abay*) using the RQUNT method in the R software package 'qmap' developed by the Norwegian Meteorological Institute [52].

2.5. Evaluations of CMIP6 Models

The skill of the 12 bias corrected CMIP6 models over the UBNB (*Abay*; 1981–2010) against the reanalysis and monthly observations were evaluated through four error metrics: the root mean square error (RMSE), the percent of bias (PBIAS %), Coefficient of Determination (R^2) and Nash–Sutcliffe Efficiency (NSE). In addition to these error metrics, a Taylor diagram was used to graphically describe how closely the patterns match ground observations [9]. It considers three error metrics including correlation coefficient, centered (unbiased) RMSE, and standard deviation in a single diagram to describe the temporal performance of climate models to the monthly observation and the reanalysis [53]. Finally, from those bias-corrected CMIP6 models, the best performing models were selected for future climate projection for the basin.

2.6. Future Climate Projection and Trend Analysis

For future climate projections, the monthly mean maximum temperature and monthly mean precipitation data were analyzed over 30-year time intervals for the baseline period (1981–2010), the near term (2031–2060), and the long term (2071–2100). The significance of temperature and precipitation trends were then examined for a continuous period from 2031 to 2100 through the non-parametric Mann–Kendall (MK) trend test method using the R "trend" package [54,55]. Non-parametric methods provide an alternative series of statistical methods that require few assumptions to be made about the data. These methods are most often used to analyze data which do not meet the distributional requirements of parametric methods. In particular, skewed data are frequently analyzed by non-parametric methods; [56] showed that the parametric-test has less power than the non-parametric Mann–Kendall test.

The Mann-Kendall (MK) test is a non-parametric test for identifying trends in time series data. To apply non-parametric MK test, the data time series does not need to be normally distributed, but it must be serially independent and randomly ordered. The test compares the relative magnitudes of sample data rather than the data values themselves [57]. Prior to the trend analysis, Statistical tests were used to examine the normality and auto-correlation of the data.

The presence of a statistically significant trend is determined using the Z-value. This statistic is used to test the null hypothesis of no trend exists against the alternative hypothesis that a trend does exist. A positive Z-value indicates an increasing trend in the time-series, while a negative Z-value indicates a decreasing trend. In this study, the significance levels of high (0.01), medium (0.05), and low (0.1) were applied, and the significant level p-value was obtained for each analyzed time-series.

3. Results

3.1. Data Checking

Climatic Research Unit (CRU TS 4.04), Global Precipitation Climatology Centre (GPCCv2020), European Community Medium-range Weather Forecasts v5 (ECMWF-ERA5), NOAA-Climate Forecast System Reanalysis v2 (CFSR), and NASA Modern Reanalysis Evaluation (NASA-MERRA v2) validation using area-averaged of 21 UBNB stations observations for the baseline period (1981–2010) show that observational temperature data from the ECMWF-ERA5 (RMSE = 1.14, r^2 = 0.88 and NSE = 0.76) and precipitation data from the GPCC.25 (RMSE = 76.21, r^2 = 0.92 and NSE = 0.76) have best agreements with the UBNB area-averaged ground observation as shown in Table 2 and Figure 2. As shown in Figure 2a MERRA reanalysis precipitation over estimates in the rainy season and CFSR temperature over estimates temperature throughout the year.

Table 2. Monthly observations and reanalysis maximum temperature and precipitation validation with UBNB area-averaged ground observations for the baseline period (1981 to 2010).

Monthly Observations and Reanalysis	ERA 5	CRU TS4.04	MERRA	CFSR	GPCC.25
Temperature (°C)					
RMSE	**1.14**	1.19	6.10	2.82	
Corr. Coeff (r^2)	**0.88**	0.86	0.62	0.85	
NSE	**0.70**	0.67	−7.50	−2.28	
Precipitation (mm/Month)					
RMSE	80.34	79.09	117.84	116.34	**76.21**
Corr. Coeff (r^2)	0.86	0.88	0.85	0.49	**0.92**
NSE	0.73	0.76	0.18	0.40	**0.76**

The temperature and precipitation climatology were computed using the ECMWF-ERA5 and GPCC.25 datasets, respectively, for the period 1981–2010. The spatial distribution of mean annual maximum temperature (°C) and precipitation (mm/day) climatology over the UBNB (*Abay*) is shown in Figure 3a,b.

3.2. CMIP6 Climate Models Bias Correction

The performance or suitability of non-parametric quantile mapping using empirical quantiles (QUANT), robust empirical quantiles (RQUANT), and smoothing-splines (SSPLIN) were checked for the dozen CMIP6 models' precipitation versus GPCC monthly observational datasets in order to use appropriate methods for bias correction. The Nash–Sutcliff efficiency (NSE) and mean absolute error (MAE) values between the observed and the corrected empirical cumulative distribution function (CDF) showed that most of them are capable to remove biases in CMIP6 models' precipitation. Figures A1–A5 reveals that the fitted quantile-quantile plots of all CMIP6 models versus observed precipitation (GPCC) and temperature (ERA5) achieve a good fit. Therefore, based on the highest NSE and lowest MAE value as shown in Table A1 the robust empirical quantiles (RQUANT) method was selected and employed as most suitable for reducing biases in CMIP6 climate models over the UBNB.

3.3. Performance Evaluation of CMIP6 Models at Regional Scale

The performance of CMIP6 models under different shared socio-economic pathways (SSPs) were evaluated in simulating future climate variables (precipitation and temperature) in the UBNB (*Abay*) based on efficiency criteria found under "hydroGOF" R package [58]. The efficiency criteria's include the root-mean-square errors (RMSEs), normalized root-mean-square errors (NRMSE), percent of bias (PBIAS), ratio of observed and simulated standard deviation (rSD), Nash–Sutcliff efficiency (NSE), and R^2. Results revealed that except UKESM1-0-LL, the remaining CMIP6 models were able to simulate the basin's major climate variables.

Dozen CMIP6 climate models evaluation with monthly observation ECMWF ERA5 and GPCC for the baseline period (1981–2010) shows that BCC-CSM-2MR (RMSE-25.66, NRMSE-27.1, PBIAS-16.4, rSD-1.17, NSE-0.93, and r^2-0.98) for precipitation and MRI-ESM2-0 (RMSE-0.74, NRMSE-32, PBIAS-(−0.9), rSD-0.75, NSE-0.90, and r^2-0.92) for temperature thereby identified certain CMIP6 models for use in UBNB (*Abay*) future climate projection as shown in Table 3.

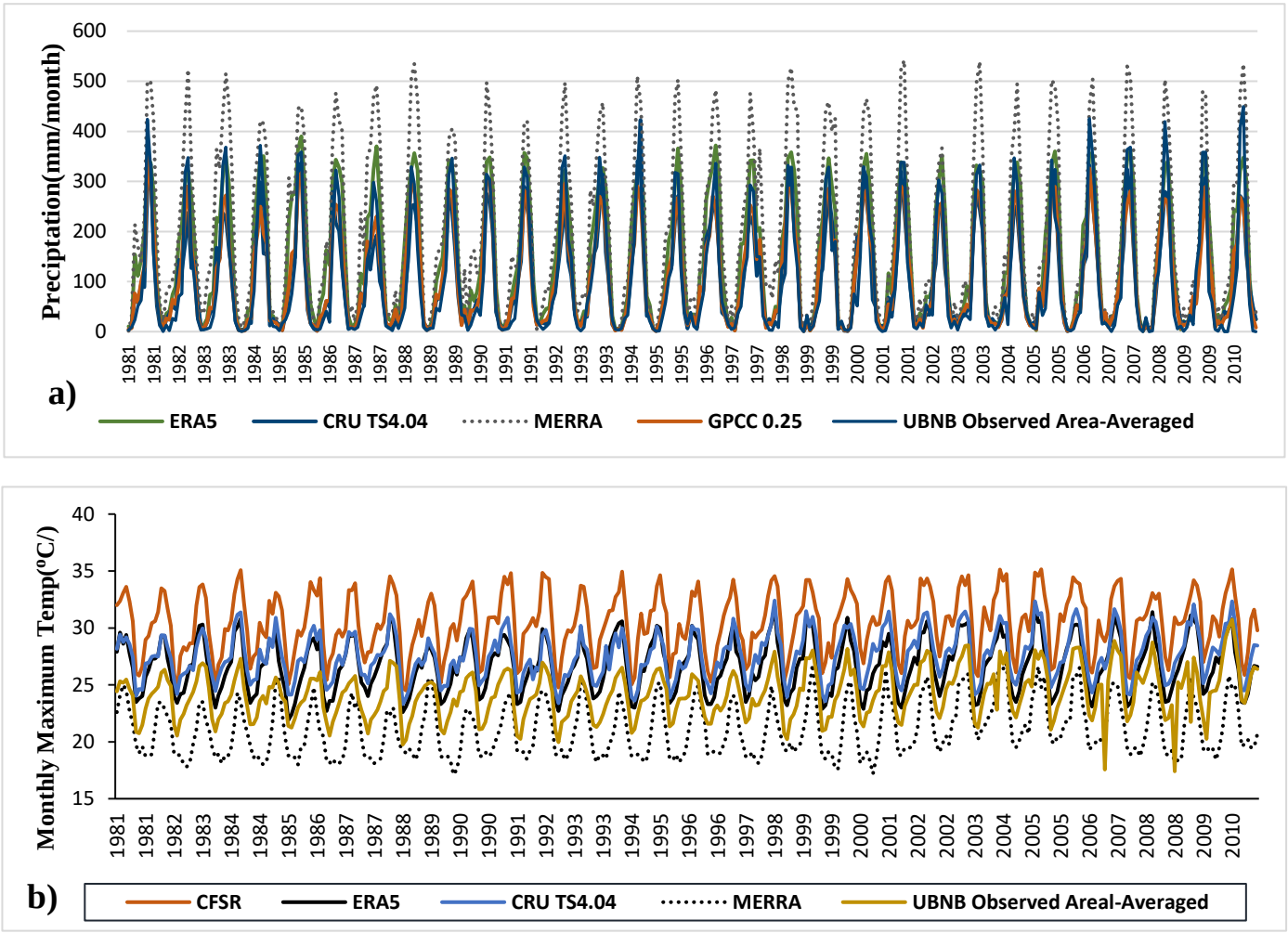

Figure 2. Temporal distribution of monthly observation and reanalysis of (**a**) precipitation (mm/month), (**b**) max. temperature (°C/month) within the Upper Blue Nile basin area-averaged.

A Taylor diagram can provide a comprehensive visualization of how well datasets relate to each other in terms of the correlation coefficient (CC) and the standard deviation. Figure 4 shows that most of CMIP6 evaluated models effectively capture the temporal changes in maximum temperature over the basin. Of these, MRI-ESM2-0, BCC-CSM2-MR, and CanESM5p1 maximum temperature outperformed, as presented by the shorter distances from the red and brown overlapped point (the observed and ECMWF-ERA5 maximum temperature data). MRI-ESM2-0 showed the shortest distance which indicated the largest CC and the lowest standard deviation compared to the observed ground and ECMWF-ERA5 maximum temperature data series. By contrast, the CanESM5p2, FGOALS-g3, MIROC6, MIROC-ES2L, and UKESM1-0-LL products showed either the lower CC or the larger standard deviation, indicating their poor performances on capturing the temporal temperature changes. Taylor diagram for precipitation in Figure 5 shows BCC-CSM2-MR outperformed, as presented by the shorter distances from the red and brown overlapped point (the observed and GPCC precipitation). Relative to CESM2, MIROC6 and UKESM1-

0-LL products CAMS-CSM1-0, CanESM5p1, CanESM5p2, CESM2-WACCM, FGOALS-g3, MCM-UA-1-0f2, MIROC-ES2L, and MRI-ESM2-0 captured the temporal changes in precipitation over the basin. On the other side, CESM2, MIROC6, and UKESM1-0-LL products showed undesired performances in capturing temporal precipitation changes, as presented by their larger distances from the observed and GPCC overlapped points.

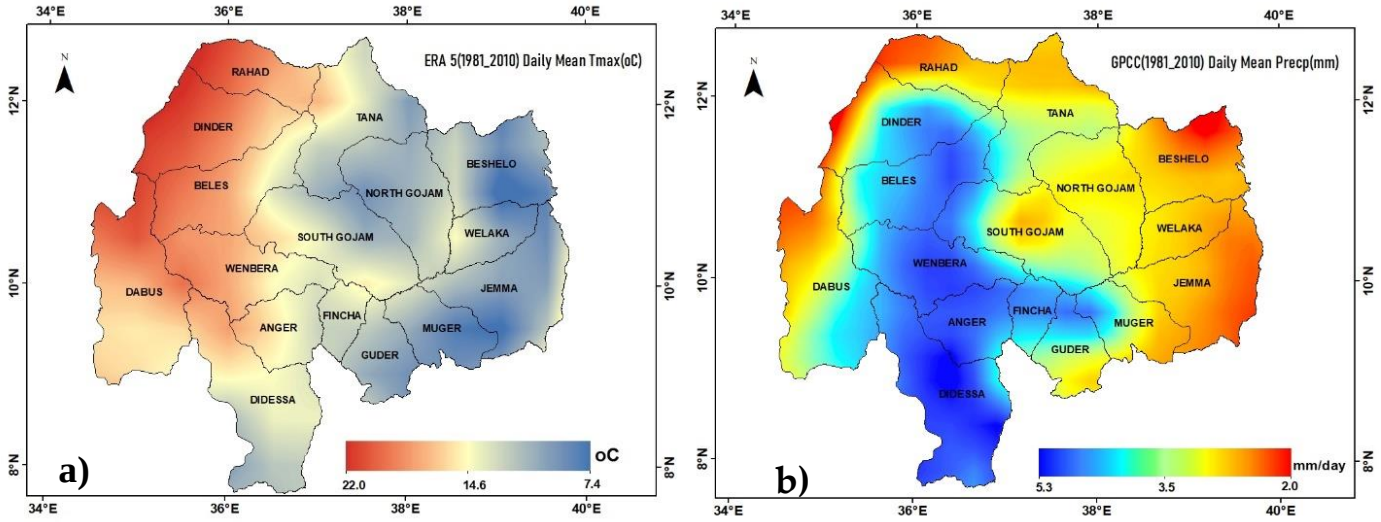

Figure 3. Spatial distribution of (**a**) ECMWF-ERA5 mean annual max. temperature (°C) and (**b**) GPCC precipitation (mm/day) climatology over the basin.

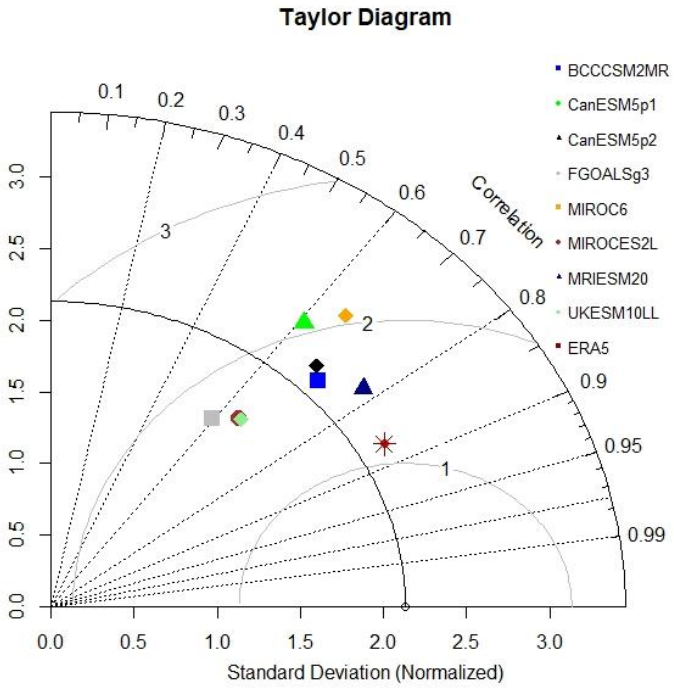

Figure 4. Taylor diagram comparing the temporal performances of nine CMIP6 models maximum temperature (°C) against the ground-observed and ECMWF-ERA5 reanalysis for the baseline period (1981–2010).

Table 3. Twelve CMIP6 models precipitation and temperature evaluation with observed GPCC and ECMWF-ERA5 using statistical parameters.

Models	RMSE	PBIAS %	NSE	R^2
Precipitation (mm/month)				
BCC-CSM-2MR	**25.66**	**16.4**	**0.93**	**0.98**
CAMS-CSM1-0	57.66	−39.4	0.63	0.96
CanESM5p1	32.51	10.5	0.88	0.98
CanESM5p2	32.97	9.8	0.88	0.98
CESM2 C	56.01	38.4	0.65	0.98
ESM2-WACCM	64.02	42.1	0.54	0.96
FGOALS-g3	49.8	22.2	0.72	0.96
MCM-UA-1-0f2	96.38	49	−0.04	0.85
MIROC6	113.2	83.5	−0.43	0.96
MIROC-ES2L	48.77	37.9	0.73	0.96
MRI-ESM2-0	35.26	26.4	0.86	0.98
UKESM1-0-LL	3236.65	1919.8	−1168.9	0.90
Temperature (°C)				
BCC-CSM2MR	1.54	5	0.55	0.92
CanESM5p1	2.21	8.1	0.08	0.94
CanESM5p2	1.79	6.4	0.4	0.90
FGOALS-g3	0.81	0.9	0.88	0.92
MIROC6	1.48	5.1	0.59	0.94
MIROC-ES2L	1.82	−6.1	0.38	0.86
MRI-ESM2-0	**0.74**	**−0.9**	**0.9**	**0.92**
UKESM1-0-LL	3.06	11.6	−0.76	0.98

Bold values are selected model highest performance values for statistical parameters.

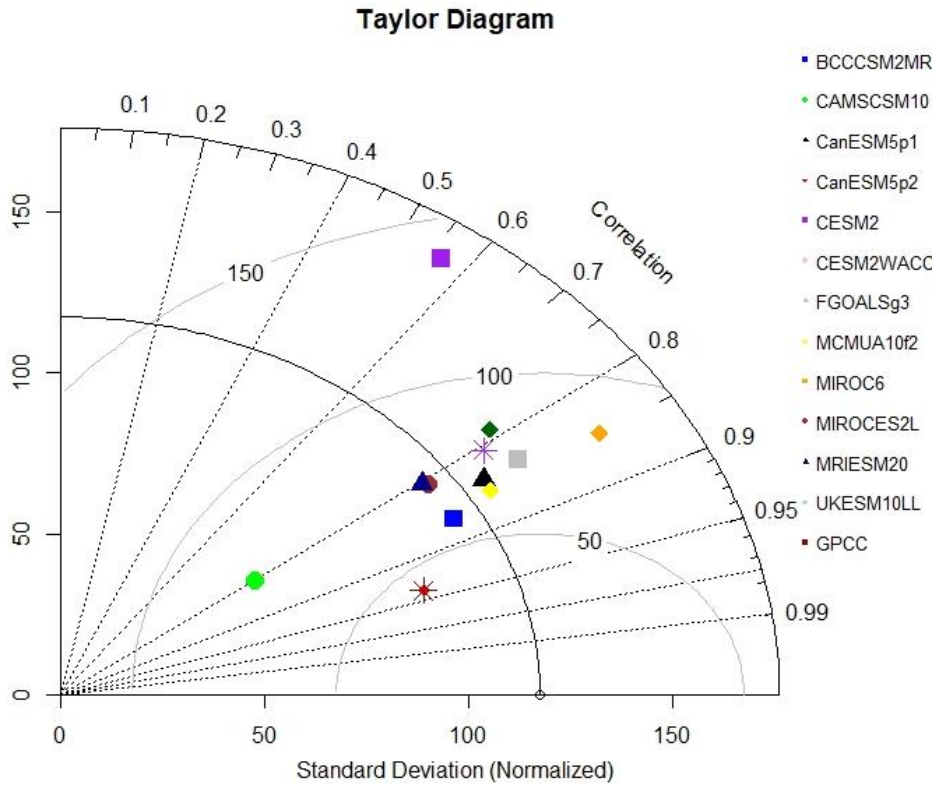

Figure 5. Taylor diagram comparing the temporal performances of twelve CMIP6 models precipitation (mm/day) against the ground-observed and GPCC reanalysis for the baseline period (1981–2010).

3.4. Future Precipitation and Temperature Trend Analysis

The nonparametric Mann–Kendall trend test was performed in R studio. The annual mean time series of MRI-ESM2-0 maximum temperature for SSP1-2.6, SSP2-4.5, SSP3-3.7, and SSP4-8.5 scenarios shows an increasing trend with Z value of (2.74, 6.36, 9.16, and 9.98) and *p*-value of 0.006 (medium), <0.002 (high), <0.002 (high), and <0.002 (high) significance levels respectively. During the twenty-first century, a continuous warming is projected as shown in Figure 6. The increasing trend in temperature over the UBNB (*Abay*) under SSP1-2.6, SSP2-4.5, SSP3-3.7, and SSP5-8.5 is projected to be 1.32 °C, 1.73 °C, 2.02 °C, and 2.6 °C, respectively. For the near (long)-term period, projected warming under SSP1-2.6, SSP2-4.5, SSP3-3.7, and SSP4-8.5 scenario is 1.1 (1.5) °C, 1.3 (2.2) °C, 1.2 (2.8) °C, and 1.5 (3.8) °C respectively.

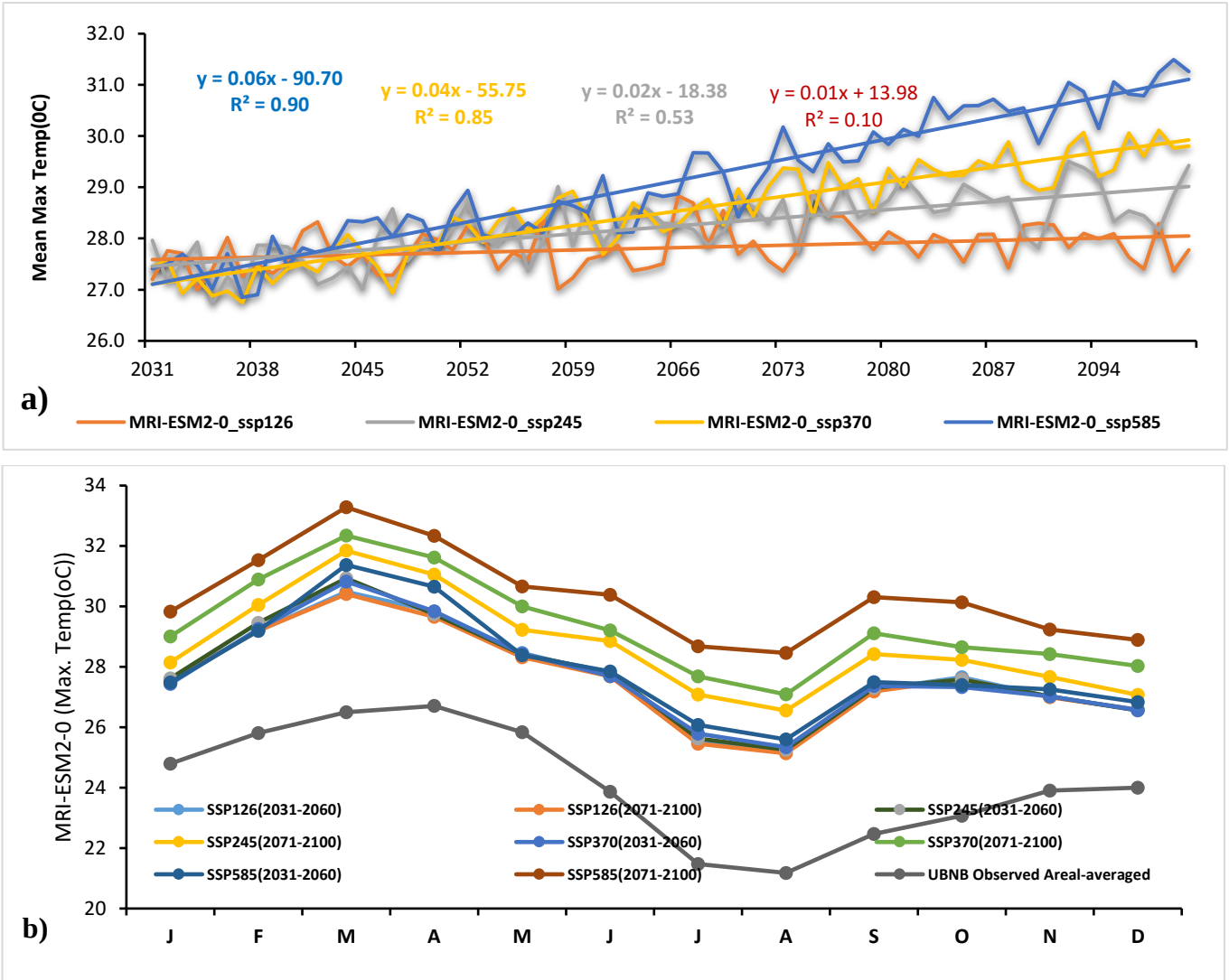

Figure 6. MRI-ESM2-0 model projections under SSP126, SSP245, SSP370, and SSP585 scenario for two future eras (2030s, 2070s). (**a**) Monthly mean max. temperature (°C) and (**b**) mean max. temperature (°C) mean annual cycle.

The trend tests of CMIP6 (BCC-CSM-2MR) precipitation projection in the rainy season JJAS (June, July, August and September) for the period 2031–2100 under SSP1-2.6, SSP2-4.5, SSP3-3.7, and SSP4-8.5 scenarios also shows positive Z-statistics of 0.10, 0.45, 2.30, and 0.87 with P-values 0.92 (low), 0.65 (low), 0.02 (high), and 0.3832 (low) significance levels respectively. The basin (*Abay*) also shows a slightly increasing (insignificant) seasonal precipitation trend of the near (long)-term period for SSP1-2.6, SSP2-4.5, SSP3-3.7, and SSP4-

8.5 with 5.9 (6.1)%, 12.8 (13.7)%, 9.5 (9.1)% and 17.1(17.7)% (See Figure 7). The projected rainy season precipitation increments during the twenty first century are 14.4 mm, 30.5 mm, 31.8, and 46.4 mm under SSP1-2.6, SSP2-4.5, SSP3-3.7, and SSP4-8.5, respectively.

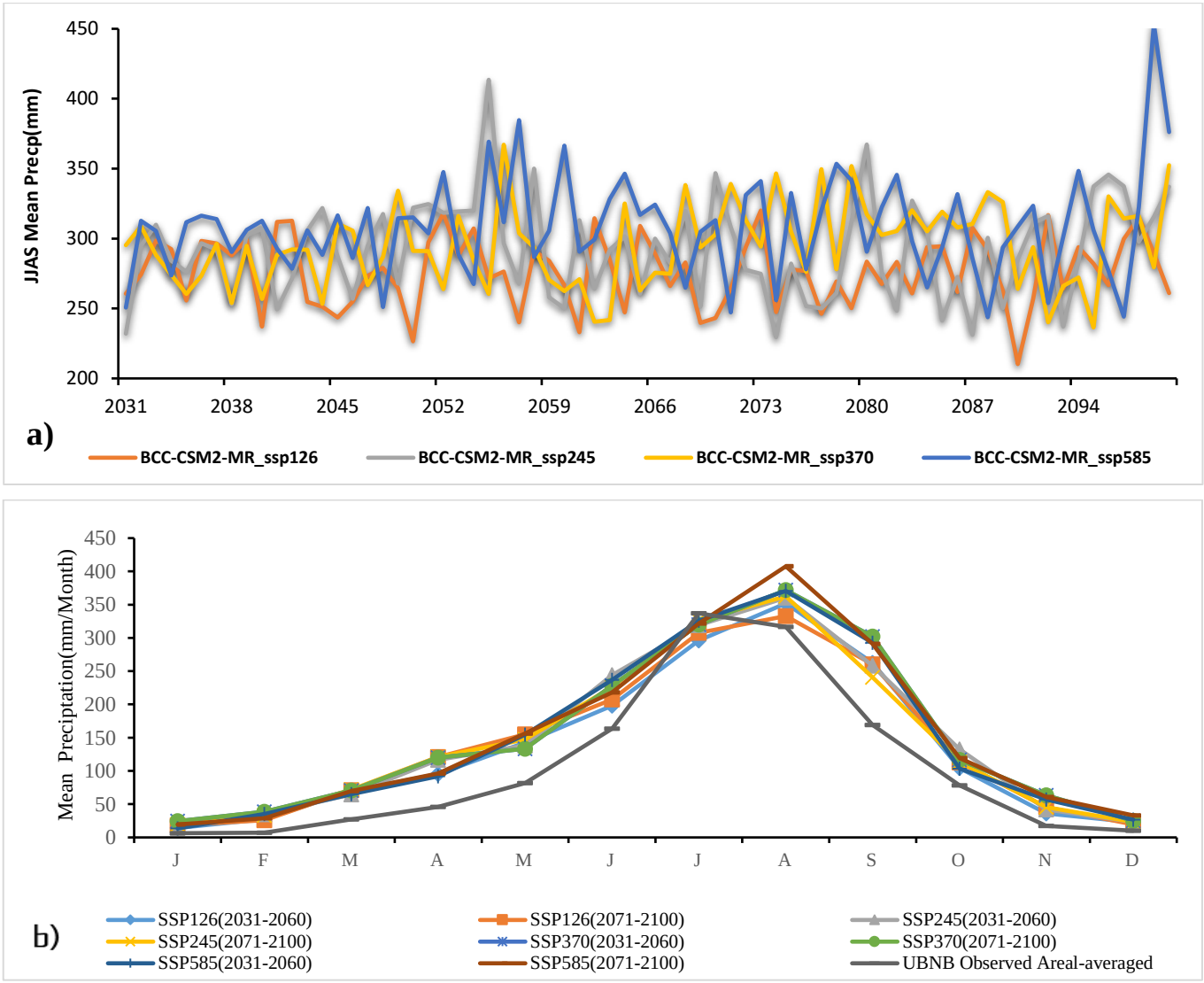

Figure 7. BCC-CSM-2MR model projections under SSP126, SSP245, SSP370 and SSP585 scenario for two future eras (2030s, 2070s). (**a**) Rainy season (JJAS) mean precipitation (mm/month). (**b**) Monthly mean precipitation mean annual cycle.

For all scenarios of BCC-CSM-2MR precipitation and MRI-ESM2-0 maximum temperature trend test, it is noted that the rainy season (JJAS) precipitation shows increasing trend with low significance level except SSP3-3.7 whereas, the annual maximum temperature trend shows an increasing trend with statistically high significance level except in the low forcing scenario (SSP1-2.6) as shown in Table 4.

3.5. Spacial Distribution of Future Precipitation and Temperature

The spatial distribution of projected changes in mean annual maximum temperature of MRI-ESM2-0 for SSP1-2.6, SSP2-4.5, SSP3-3.7, and SSP4-8.5 scenarios over the basin has shown similar spatial distribution with the observed ERA5. Relative to the baseline (1981–2010) climate, the future temperature projections indicate enhanced warming over the basin under all future scenarios except the low forcing scenario (SSP1-2.6) during both the near and long-term periods. The warming is more pronounced in the northeastern parts

of *Abay* basin relative to the southwestern part for both the near and long-term projections. (Figures 8 and A6).

Table 4. Changes in mean annual maximum temperature and mean annual precipitation by the end of century (2071–2100) relative to the baseline period (1981–2010) in the UBNB (*Abay*).

RCM Runs	Time	Scenarios			
BCC-CSM-2MR Mean Precipitation (mm/Month)		**SSP1-2.6**	**SSP2-4.5**	**SSP3-7.0**	**SSP5-8.5**
	Baseline	261.8	261.8	262.9	261.8
	2031–2060	277.13	295.4	287.87	306.55
	2071–2100	277.79	297.60	286.89	308.26
	2031–2100	276.19	292.33	294.71	308.23
	Change of 21th Century (%)	5.5	11.7	12.1	17.7
	Change of Near-term (%)	5.9	12.8	9.5	17.1
	Change of Long-term (%)	6.1	13.7	9.1	17.7
MRI-ESM2-0 Max. Temperature (°C)		**SSP1-2.6**	**SSP2-4.5**	**SSP3-7.0**	**SSP5-8.5**
	Baseline	26.5	26.5	26.5	26.5
	2031–2060	27.6	27.8	27.7	28
	2071–2100	28.0	28.7	29.3	30.3
	2031–2100	27.8	28.2	28.5	29.1
	Change of 21th Century (°C)	1.3	1.7	2.0	2.6
	Change of Near-term (°C)	1.1	1.3	1.2	1.5
	Change of Long-term (°C)	1.5	2.2	2.8	3.8

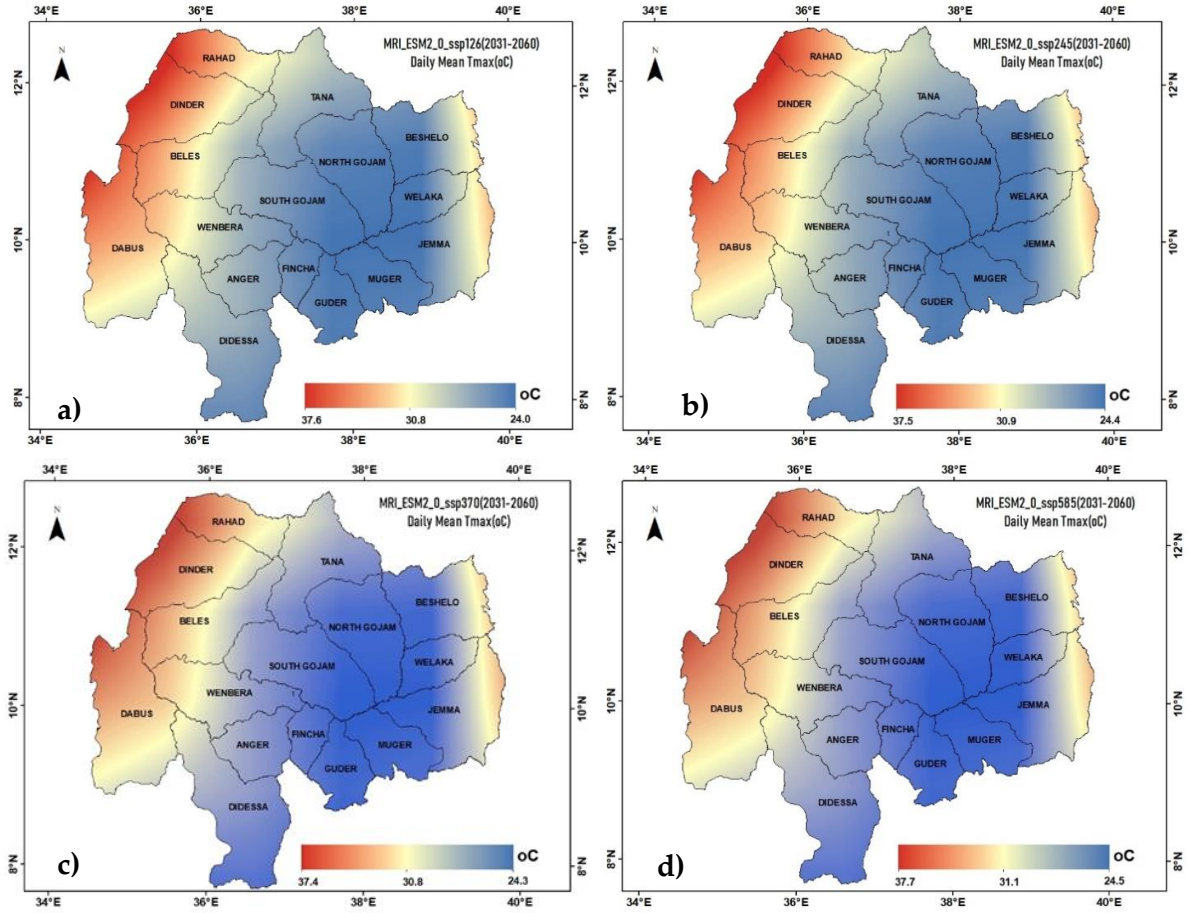

Figure 8. Spatial distribution of CMIP6-MRI-ESM2-0 model daily mean maximum temperature (°C) for (**a**) SSP126(24–37.6), (**b**) SSP245(24.4–37.5), (**c**) SSP370(24.3–37.4), and (**d**) SSP585(24.5–37.7) scenarios over the UBNB for the near-term projections (2031–2060). The spatial distributions of daily mean maximum temperature for four SSP scenarios looks identical but the range of the value are different.

The spatial distribution of projected changes in rainy-season (JJAS) mean precipitation of BCC-CSM-2MR for SSP1-2.6, SSP2-4.5, SSP3-3.7 and SSP4-8.5 scenarios over the basin is shown to have a similar distribution with the observed GPCC. The future precipitation projections indicate wetter conditions over the basin under all future scenarios except the medium to high forcing scenario (SSP3-3.7) during both the near and long-term periods. The bilinear interpolated spatial distribution of changes in precipitation over the basin is shown in Figures 9 and A7 for near and long-term projection of BCC-CSM-2MR; SSP1-2.6, SSP2-4.5, SSP3-3.7, and SSP4-8.5 scenarios. The precipitation pattern shows a slight reduction over the northern, east, and west parts of the basin, and an increase in the southern parts, during both the near and long-term periods under the four scenarios. The projected change shows lower precipitation over the northern, east, and west parts as compared with the southern parts.

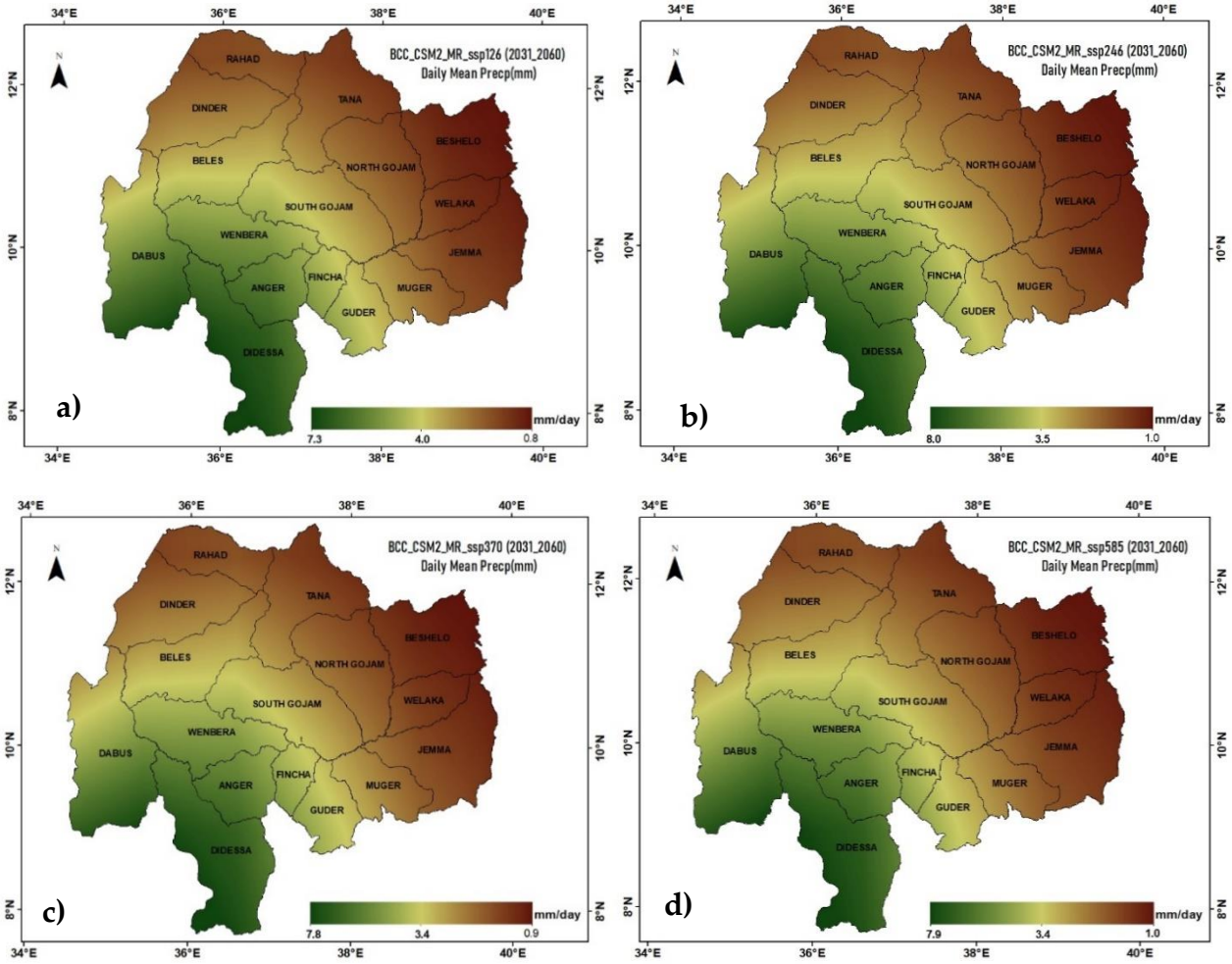

Figure 9. Spatial distribution of CMIP6-BCC-CSM2-MR model daily mean precipitation(mm/day) for (**a**) SSP126 (0.8–7.3), (**b**) SSP245(1.0–8.0), (**c**) SSP370 (0.9–7.8), and (**d**) SSP585 (1.0–7.9) scenarios over the UBNB for the near-term projections (2031–2060). The spatial distributions of mean precipitation for four SSP scenarios looks identical but the range of the value is different.

4. Discussions

4.1. Baseline Validation and Bias Correction

Climate modeling using GCMs/RCMs over the complex topography of UBNB needs systemic error reduction in every step of investigation. Several previous works considered CRU, NCEP/CFSR, NCEP/NCAR, GPCC, ERA-interim, and GPCP reanalysis and monthly observation to depict baseline period climatology for climate prediction of the UBNB [8,12,17,31,59,60]. In most studies, the reanalysis and monthly observation products

were applied directly without validating with ground observational data. In this study, dataset validation is done using area-averaged over 21 UBNB stations observations for the baseline period (1981–2010). Statistical measures showed that reanalysis temperature data from the ECMWF-ERA5 with RMSE (1.14), R^2 (0.88), NSE (0.70), and precipitation data from the GPCC.25 with RMSE (76.21), R^2 (0.92), NSE (0.76) are steadiest than the remaining products as shown in Table 2. This increases the level of confidence on model selection and climate projection of the basin.

Quantile mapping suitability checkup demonstrates that apart from DIST, PTF, and SSPLIN, the rest of the considered QM methods can provide relatively improved results for both rainfall and temperature variables for the basin (*Abay*). The robust empirical quantiles (RQUANT) methods proved to be excellent options to correct the bias of rainfall data, from all bias correction methods. In a comprehensive inter-comparison study of seven empirical statistical downscaling and error correction methods for daily precipitation, quantile mapping (QM) outperforms over all other investigation methods [61]. Similarly, [52] has also proved that area-averaged observations of 82 precipitation stations in Norway using nonparametric transformations have the highest skill in systematically reducing biases in RCM precipitation [51]. Quantile mapping methods (QUNT) comparison showed that robust quantile mapping method (RQUNT) has a good performance in reproducing evaluation criteria's like Nash–Sutcliff efficiency and mean absolute error (MAE) [51].

4.2. Model Selection and Future Climate Projection

It is subjective and difficult to select a specific model for a given study area [8]. In their study [26] proved that most of CMIP6 models are able to simulate the East African major climate variables. In this study for UBNB, twelve CMIP6 models evaluation confirmed that BCC-CSM-2MR for precipitation and MRI-ESM2-0 for temperature have excellent agreement with the baseline period observational datasets. The comparative analysis [62] of six CMIP5 model outputs showed that BCC-CSM-2MR had similar trends to the observed precipitation.

Several previous works projected the future climate of the basin using various generation of models and came up with diversified results as summarized in Table 5. Most studies project a clear increase in temperature by the end of the 21st century, in the order of 1–7 °C. On the other hand, the direction and magnitude of precipitation change in the basin at regional, basin-wide, and sub-basin scale, and is challenging to figure out. All of these studies used different periods, numbers, and types of climate models, emission scenarios, and downscaling methods which make generalizing difficult. From Table 5, changes in rainy season (JJAS) precipitation ranges between −36% and +35%. Most importantly, more than half of the reviewed studies showed a slight increasing trend over the basin which aligns with the projections of this study.

Table 5. Projected changes in temperature and precipitation by 21 previous studies in East Africa, Ethiopia, and UBNB (*Abay*).

No.	Region/Basin/Watershed	Area (km^2)	Model Runs	Time	Scenarios	Change in Max. Temp. (°C)	Change in Precip. (%)	Source
1	East Africa		23 CMIP5	**1981–2010** 2006–2100	RCP8.5		Increasing	[62]
2	East Africa	-	COSMO-CLM	**1950–2005** 2006–2100	RCP4.5 RCP8.5	3 6		[63]
3	East Africa	-	27 CMIP6	**1981–2010** 2030–2059 2070–2099	SSP1-2.6 SSP2-4.5 SSP5-8.5	1.2 (1.3) 1.3 (2.3) 1.7 (4.1)	14.2 (12.3) 16.9 (18.4) 24.5 (51)	[26]
4	Ethiopia	1.29 million	6 CMIP 5	**1971–1990** 1991–2010 2035–2054			−10.6 −17.5	[64]
5	Ethiopia	1.29 million	GFDL- GCM	**1948–2006** 2001–2050	A1B	4	−3	[12]
6	Blue Nile	3.35 million	19 CMIP5	2006–2100	RCP2.6 RCP8.5	3 6	−20 −20	[63]
7	Blue Nile	3.35 million	11 GCMs	**1950–1999** 2010–2099	A2 (B1)	1.5 (1.3)	115 (117)mm	[59]
8	Blue Nile	3.35 million	17 GCMs	2081–2098	A1	5.00	No change	[11]
9	Blue Nile	3.35 million	11 GCMs	**1950–1999**				[59]
10	Blue Nile UBNB	3.35 million 176,000	11 GCMs 3 GCM	2010–2039 2040–2069 2070–2099 2010–2039 2040–2069 2070–2099	A2 (B1) A2 B2	1.5(1.3) 3.2(2.8) 4.4(3.6)	115 (117)mm 98 (104) mm 93 (96) mm −8.8 23.30 54.60	[28]
11	UBNB	176,000	COSMO-CLM	**1981–2010** 2070–2099	RCP4.5 RCP8.5	2.48 4.89	−10.8 −19.0	[60]
12	UBNB	176,000	11 GCMs	2070–2099			−24.0	[59]
13	UBNB	176,000	3 CMIP3	**1979–2013** 2046–2064 2081–2099	A1B	2–2.7 2.7–3.7	17.42–46.12 7.73- 48.44	[17]
14	UBNB	176,000	5 CMIP 5	**1971–2000** 2041–2070	RCP4.5		Decreasing	[65]
15	UBNB	176,000	ECHAM5 GCM	**1961–1990** 2011–2040 2015–2030 2041–2070	A1B	8% 13.80% 23.90%	1.8 −6.6 −6.4	[66]
16	UBNB	176,000	3 GCMs	**1970–2000** 2046–2065 2081–2100	A1B A2	0.6–2.7 0.9–4.63	−36 to 1	[67]
17	UBNB	176,000	6 GCMs	**1961–1990** 2011–2040	A2	2.3	11	[32]
18	UBNB	176,000	COSMO-CLM	**1983–2100** 1971–2000	A1B	Increasing	Decreasing	[31]
19	Tana and Belse	28,549	6 CMIP5	**1979–2010** 2041–2065 2075–2099	 RCP2.6, RCP4.5 RCP6.0, RCP8.5	 8.6% (15.7%) 2.4% (21.2%)	 11.0(17.6) 11.7(18.4)	[68]
20	Tana Basin	15,000	CanESM2 GCM	2011–2040, 2041–2070 2071–2100	RCP2.6 RCP8.5 RCP4.5	2.14	25	[69]
21	Tana basin	15,000	5 CMIP5	2035–2064 2071–2100	RCP 4.5 RCP 8.5	3.9 7.1	−8.9 to 25.2 −10.8 to 34.4	[19]

Bold values are baseline periods for projections.

From these studies, recently [60] mean annual maximum (minimum) temperature projection showed an increasing trend by 2.48(4.74) °C under RCP4.5 and 4.89(2.22) °C under RCP8.5 by the end of the 21st century (2070–2099). Similar warming trends of mean annual temperature with large seasonal and spatial variations over the basin were also reported by other studies e.g., [11,12,17,28,59,60,63,65–69].

Refs. [17,70] found increasing trends of mean annual rainfall up to 27%. Unlike [69,71] reported an increasing trend during the rainy season and no significant trend during the dry season. An increasing tendency for extreme precipitation event contributions to total precipitation for East Africa was reported by [26,61]. Refs. [62,71] also stated that precipitation over Africa is expected to become more concentrated and intense. Recent study by [26] using CMIP6, North East Africa (NEAF) region shows an increasing precipitation trend in SSP5-8.5, while SSP2-4.5 and SSP1-2.6 had no uniform trend during these periods. However, several climate change studies showed that precipitation projections are full of uncertainty [72,73]. For instance, on the contrary of all the above results, [60], [67] reported declining trends of mean annual precipitation up to −10.8% under RCP4.5 and −19.0% under RCP8.5 by the end of the century. In some studies, non-linear trends emerged: warming increases toward the end of the twenty-first century, especially in the high-emission SSP5-8.5 scenario. Recently, [26] reported maximum temperature increment trends for all implemented scenarios of CMIP6 over "North East Africa (NEAF)" as defined in the IPCC's sixth assessment [74].

In general, the tenable reasons that specific unified trends were not detected in the previous studies are the higher variability of rainfall in the UBNB, complex topography of the basin, insufficiency in the number of analyzed data for the extraction of a long-term trend, and different statistical measures used in each study.

5. Conclusions

Climate predictions using recent and high-resolution climate models are becoming important for effective decision-making and suitable adaptation strategies. The Nile River faces competing water resource demands, which in turn, require a sufficient understanding of the climate and hydrological processes at basin scale. This study discusses, the past and future climate under the sixth phase of the Coupled Model Intercomparison Project (CMIP6) Shared-socio-economic pathways (SSPs) scenarios projection for UBNB (*Abay*).

The findings in this study revealed that, ECMWF-ERA5 for temperature and GPCC for precipitation have best agreement with the ground observational data for the baseline period (1981–2010), RQUNT transformation had the highest skill in systematically reducing biases in CMIP6 models precipitation and temperature. In the twenty-first century, MRI-ESM2-0 mean annual maximum temperature under the Shared Socioeconomic Pathways (SSPs) for low, medium, medium to high, and strong forcing, referenced as SSP1-2.6, SSP2-4.5, SSP3-3.7, and SSP5-8.5 trend test showed the expected warming trend over the basin.

On the other hand, the BCC-CSM-2MR precipitation projections show slightly increasing trend under all the Shared Socioeconomic Pathways (SSPs): SSP1-2.6, SSP2-4.5, SSP3-3.7, and SSP5-8.5. The spatial distribution of the rainy season precipitation showed reduction from south to north while the maximum temperature shows increment from east to west.

The data and results contained herein can be used to estimate the uncertainty in future precipitation and temperature and to predict future hydro-meteorological variables of the basin. This study is one of the initial assessments of a CMIP6 climate models over UBNB (*Abay*) in which a large number of climate models have been employed. It offers useful information about the basin patterns of projected temperature and precipitation. In general, according to the model's projection the basin will most likely benefit from the evident climate change in this century.

Author Contributions: Conceptualization, A.A.A., S.A.T., S.A.L., F.A.Z., G.B.T. and M.R.J.; A.A.A. analyzed the data and drafted the manuscript; F.A.Z. revised the statistical results; All authors contributed to editing and organizing the manuscript; supervision, M.R.J., S.A.T. All authors have read and agreed to the published version of the manuscript.

Funding: The first author would like to thank School of Research and Graduate Studies, Bahir Dar Institute of Technology, Bahir Dar University for providing financial support for PhD research work.

Institutional Review Board Statement: Not applicable.

Informed Consent Statement: Not applicable.

Data Availability Statement: Data used in this study can be accessed from the KNMI Climate Explorer Website: https://climexp.knmi.nl/start.cgi (accessed on 24 July 2021), the World Climate Research Programmer's WCRP Website: https://www.wcrp-climate.org/, accessed on 24 July 2021, The Ethiopian National Meteorological Agency Website: http://www.ethiomet.gov.et/, accessed on 24 July 2021 and The Ethiopian Ministry of Water Irrigation and Energy, Website: http://mowie.gov.et/, accessed on 24 July 2021.

Acknowledgments: The Ethiopian National Meteorological Agency provided climatic data. We recognized the World Climate Research Programme's Working Group on Coupled Modelling and all the modelling groups that performed the simulations and made their data available. Reanalysis, Monthly Observation and CMIP6 results are openly available through the KNMI Climate Explorer Website: https://climexp.knmi.nl/start.cgi (accessed on 24 July 2021).

Conflicts of Interest: The authors declare no conflict of interest.

Appendix A

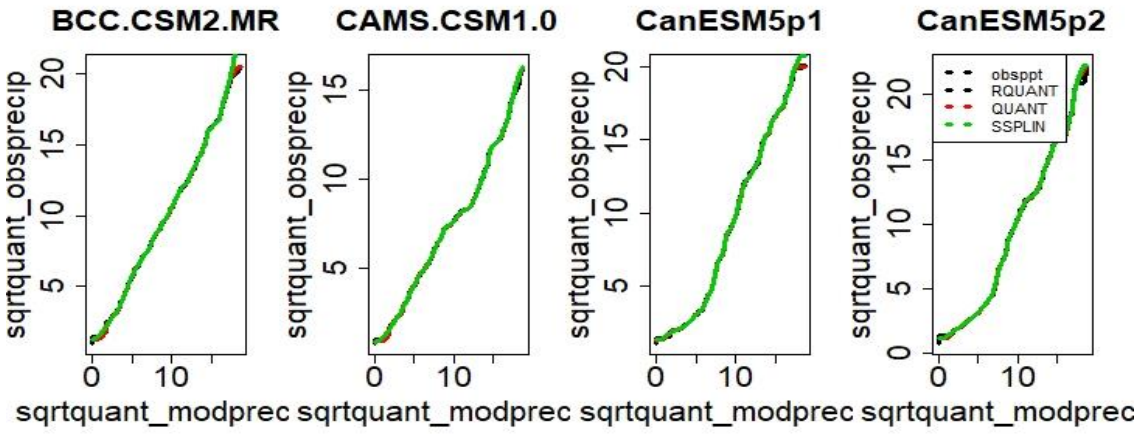

Figure A1. Square root quantile–quantile mapping of model precipitations (BCC-CSM2-MR, CAMS-CSM1-0, CanESM5p1 and CanESM5p2) versus GPCC monthly observation precipitation.

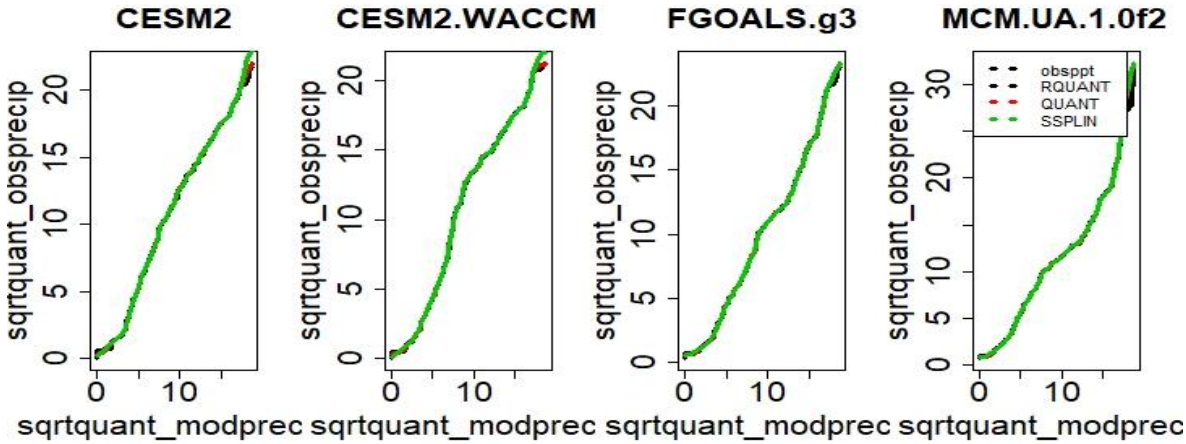

Figure A2. Square root quantile- quantile mapping of model precipitations (CESM2, CESM2-WACCM, FGOALS-g3, and MCM-UA-1.0f2) versus GPCC monthly observation precipitation.

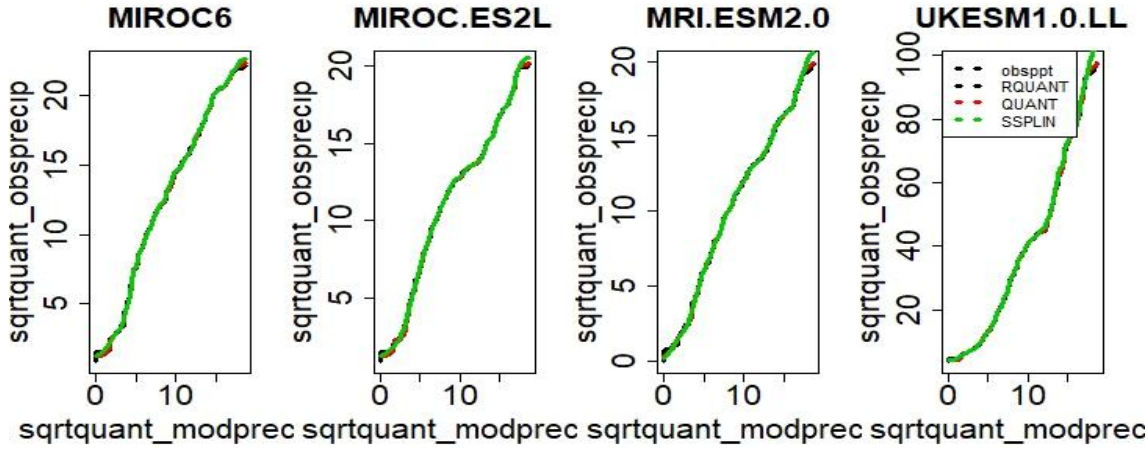

Figure A3. Square root quantile- quantile mapping of model precipitations (MIROC6, MIROC-ES2L, MRI-ESM2-0, and UKESM1-0-LL) versus GPCC monthly observation precipitation.

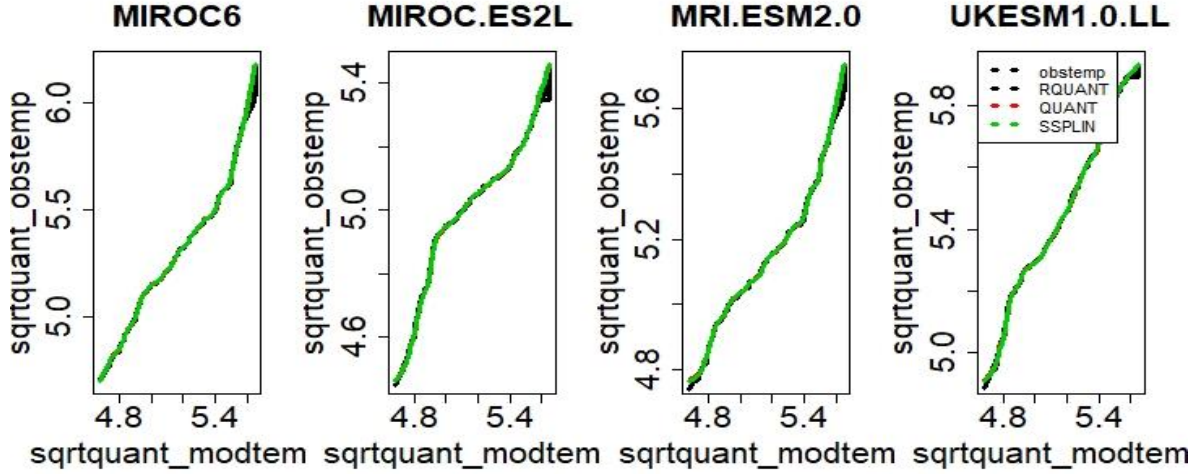

Figure A4. Square root quantile- quantile mapping of model Tmax (MIROC6, MIROC-ES2L, MRI-ESM2-0, and UKESM1-0-LL) versus ECMWF-ERA5 monthly observation.

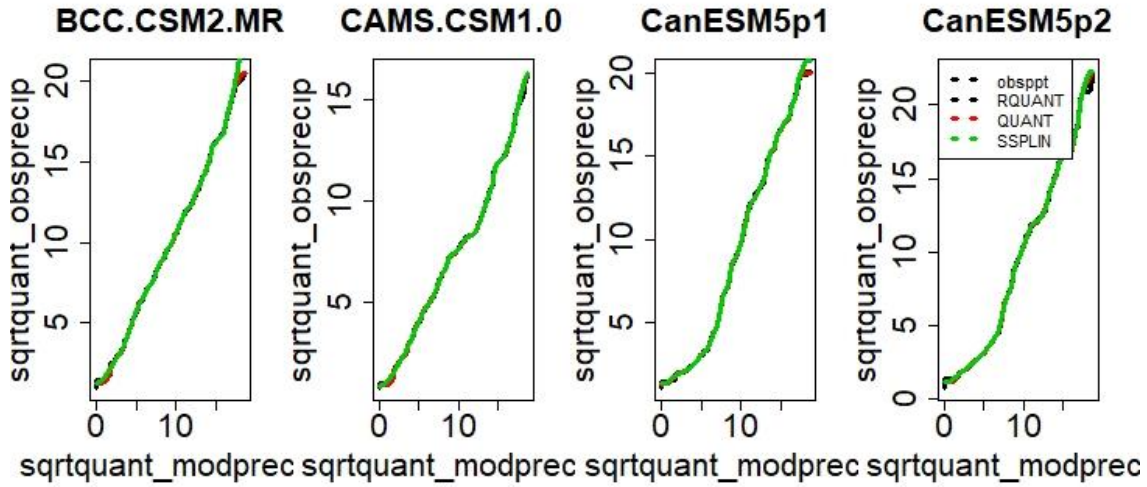

Figure A5. Square root quantile- quantile mapping of model Tmax (BCC-CSM2-MR, CanESM5p1, CanESM5p2, and FGOALS-g3) versus ECMWF-ERA5 monthly observation.

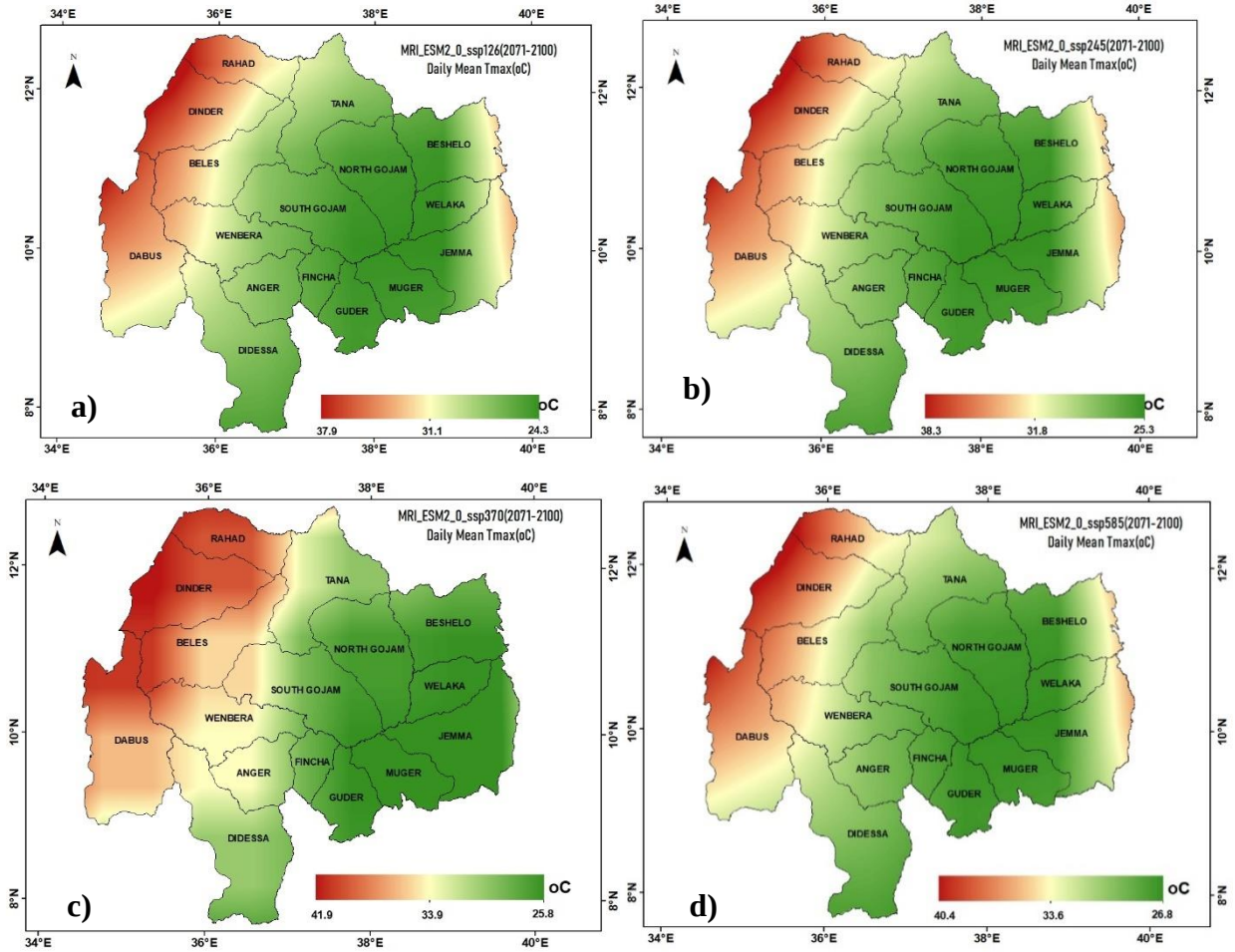

Figure A6. Spatial distribution of CMIP6- MRI-ESM2-0 model daily mean max. temperature (°C) for (**a**) SSP126(24.3–37.9), (**b**) SSP245(25.3–38.3), (**c**) SSP370(25.8–41.9), and (**d**) SSP585(26.8–40.4) scenarios over the UBNB for the long-term projections (2071–2100). The spatial distributions of mean max. temperature for four SSP scenarios looks identical but the range of the value are different.

Table A1. Non parametric quantile mapping methods performance evaluation using Nash–Sutcliff efficiency (NSE) and mean absolute error (MAE) values for bias correction.

Model PRECP	RQUANT (NSE)	QUANT (NSE)	SSPLIN (NSE)	RQUANT (MAE)	QUANT (MAE)	SSPLIN (MAE)
BCC-CSM2-MR	**0.756**	0.755	0.734	**40.402**	40.464	41.168
CAMS-CSM1-0	**0.603**	0.599	0.600	**26.400**	26.521	26.469
CanESM5p1	**0.758**	0.758	0.754	**39.235**	39.332	39.514
CanESM5p2	**0.735**	0.731	0.728	**41.812**	42.017	42.183
CESM2	**0.748**	0.748	0.740	**46.733**	46.741	47.307
CESM2-WACCM	**0.739**	0.738	0.732	**48.354**	48.436	48.790
FGOALS-g3	**0.704**	0.703	0.702	**48.700**	48.716	48.831
MCM-UA-1-0f2	**0.148**	0.110	0.104	**103.444**	104.401	104.562
MIROC6	**0.797**	0.796	0.794	**52.094**	52.162	52.512
MIROC-ES2L	**0.695**	0.694	0.693	**48.041**	48.068	48.261
MRI-ESM2-0	**0.699**	0.698	0.693	**45.319**	45.407	45.611
UKESM1-0-LL	**0.766**	0.764	0.751	**775.618**	780.088	793.310
Model TEMP						
BCC-CSM2-MR	**0.797**	0.796	0.794	**1.498**	1.509	1.508
CanESM5p1	**0.695**	0.694	0.693	**1.036**	1.044	1.042
CanESM5p2	**0.699**	0.698	0.695	**1.035**	1.039	1.039
FGOALS-g3	**0.766**	0.764	0.751	**1.005**	1.009	1.007
MIROC6	**0.797**	0.796	0.794	**1.498**	1.509	1.508
MIROC-ES2L	**0.695**	0.694	0.693	**1.036**	1.044	1.042
MRI-ESM2-0	**0.699**	0.698	0.695	**1.035**	1.039	1.039
UKESM1-0-LL	**0.766**	0.764	0.751	**1.005**	1.009	1.007

Bold values are highest performance values for NSE and MAE for RQUNT.

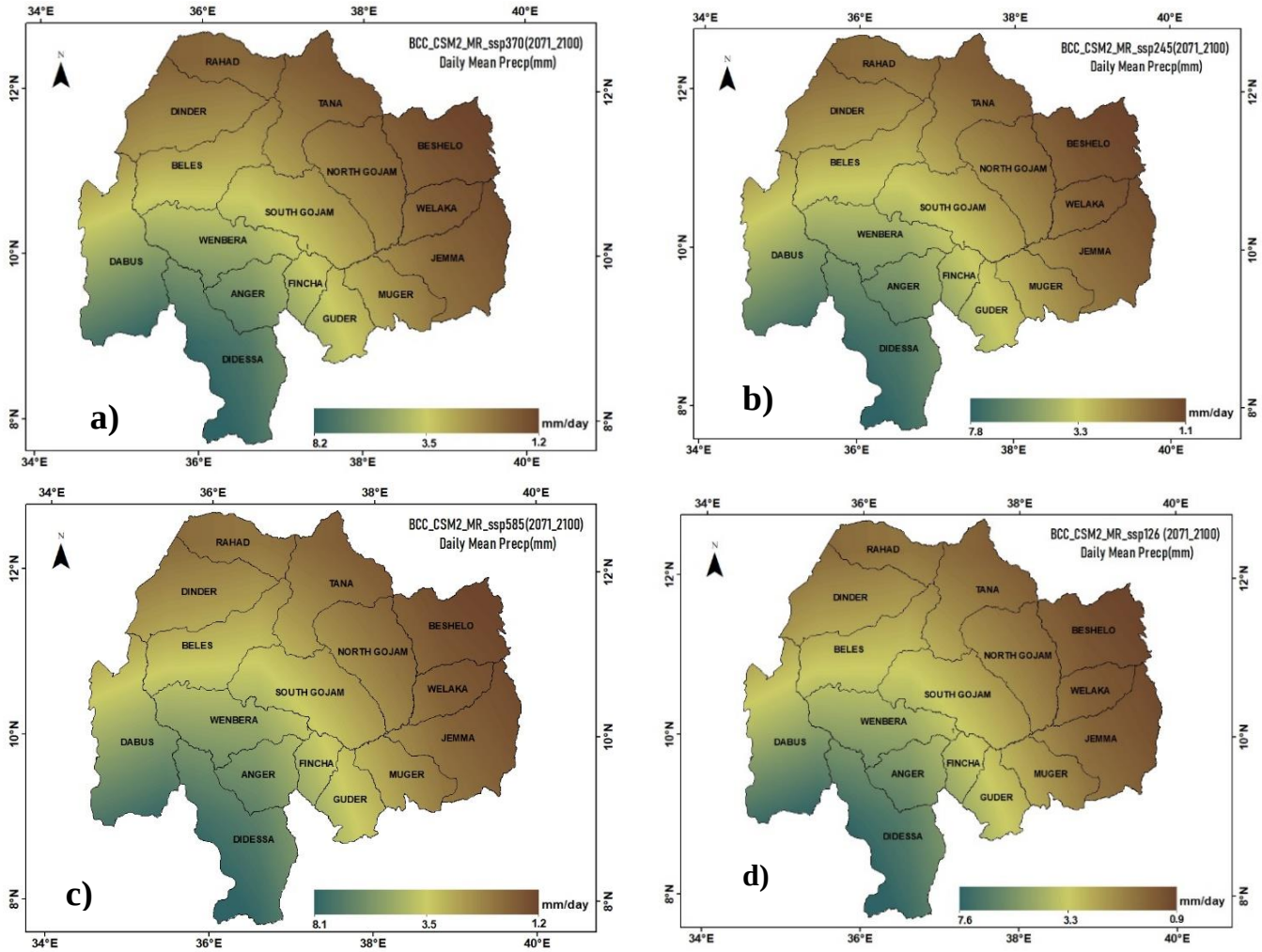

Figure A7. Spatial distribution of CMIP6-BCC-CSM2-MR model daily mean precipitation (mm/day) for (**a**) SSP126 (1.2–8.2), (**b**) SSP245 (1.1–7.8), (**c**) SSP370 (1.2–8.1), and (**d**) SSP585 (0.9–7.6) scenarios over the UBNB for the long-term projections (2071–2100).The spatial distributions of mean precipitation for four SSP scenarios looks identical but the range of the value are different.

References

1. Collier, P.; Conway, G.; Venables, T. Climate change and Africa. *Oxf. Rev. Econ. Policy* **2008**, *24*, 337–353. [CrossRef]
2. IPCC. Part A: Global and Sectoral Aspects. Contribution of Working Group II to the Fifth Assessment Report of the Intergovernmental Panel on Climate Change. Climate Change 2014. Impacts, Adaptation, and Vulnerability. 2014. Available online: https://www.ipcc.ch/site/assets/uploads/2018/02/WGIIAR5-PartA_FINAL.pdf (accessed on 24 July 2021).
3. Sutton, S.G.; Tobin, R. Constraints on community engagement with Great Barrier Reef climate change reduction and mitigation. *Glob. Environ. Chang.* **2011**, *21*, 894–905. [CrossRef]
4. Birch, E.L. A Review of "Climate Change 2014: Impacts, Adaptation, and Vulnerability" and "Climate Change 2014: Mitigation of Climate Change". *J. Am. Plan. Assoc.* **2014**, *80*, 184–185. [CrossRef]
5. Tesemma, Z.K.; Mohamed, Y.A.; Steenhuis, T.S. Trends in rainfall and runoff in the Blue Nile Basin: 1964–2003. *Hydrol. Process.* **2010**, *24*, 3747–3758. [CrossRef]
6. Dile, Y.T.; Tekleab, S.; Ayana, E.K.; Gebrehiwot, S.G.; Worqlul, A.W.; Bayabil, H.K.; Yimam, Y.T.; Tilahun, S.A.; Daggupati, P.; Karlberg, L.; et al. Advances in water resources research in the Upper Blue Nile basin and the way forward: A review. *J. Hydrol.* **2018**, *560*, 407–423. [CrossRef]
7. Addisu, S.; Selassie, Y.G.; Fissha, G.; Gedif, B. Time series trend analysis of temperature and rainfall in lake Tana Sub-basin. *Ethiopia. Environ. Syst. Res.* **2015**, *4*, 25. [CrossRef]
8. Conway, D.; Hulme, M. Recent fluctuations in precipitation and runoff over the Nile sub-basins and their impact on main Nile discharge. *Clim. Chang.* **1993**, *25*, 127–151. [CrossRef]
9. Strzepek, K.; Yates, D.; El Quosy, D. Vulnerability assessment of water resources in Egypt to climatic change in the Nile Basin. *Clim. Res.* **1996**, *6*, 89–95. [CrossRef]
10. Conway, D. The Climate and Hydrology of the Upper Blue Nile River. *Geogr. J.* **2000**, *166*, 49–62. [CrossRef]

11. Elshamy, M.; Seierstad, I.A.; Sorteberg, A. Impacts of climate change on Blue Nile flows using bias-corrected GCM scenarios. *Hydrol. Earth Syst. Sci.* **2009**, *13*, 551–565. [CrossRef]
12. Jury, M.R.; Funk, C. Climatic trends over Ethiopia: Regional signals and drivers. *Int. J. Clim.* **2012**, *33*, 1924–1935. [CrossRef]
13. Samy, A.; Ibrahim, M.G.; Mahmod, W.; Fujii, M.; Eltawil, A.; Daoud, W. Statistical Assessment of Rainfall Characteristics in Upper Blue Nile Basin over the Period from 1953 to 2014. *Water* **2019**, *11*, 468. [CrossRef]
14. Abtew, W.; Dessu, S.B. Grand Ethiopian Renaissance Dam Analysis. In *The Grand Ethiopian Renaissance Dam on the Blue Nile. Springer Geography*; Springer: Cham, Switzerland, 2019. [CrossRef]
15. Chen, H.; Swain, A. The Grand Ethiopian Renaissance Dam: Evaluating Its Sustainability Standard and Geopolitical Signifi-cance. *Energy Dev. Front.* **2014**, *3*, 11–19.
16. Soliman, G.; Soussa, H.; El-Sayed, S. Assessment of Grand Ethiopian Renaissance Dam impacts using Decision Support System. *IOSR J. Comput. Eng.* **2015**, *18*, 2278–2661. [CrossRef]
17. Roth, V.; Lemann, T.; Zeleke, G.; Subhatu, A.T.; Nigussie, T.K.; Hurni, H. Effects of climate change on water resources in the upper Blue Nile Basin of Ethiopia. *Heliyon* **2018**, *4*, e00771. [CrossRef]
18. Solomon, S.; Qin, D.; Manning, M.; Chen, Z.; Marquis, M.; Averyt, K.B.; Tignor, M.; Miller, H.L. (Eds.) *AR4 Climate Change 2007: The Physical Science Basis*; Contribution of Working Group I to the Fourth Assessment Report of the Intergovernmental Panel on Climate Change; Cambridge University Press: Cambridge, UK; New York, NY, USA, 2007.
19. Gebre, S.L.; Ludwig, F. Hydrological Response to Climate Change of the Upper Blue Nile River Basin: Based on IPCC Fifth Assessment Report (AR5). *J. Clim. Weather. Forecast.* **2015**, *3*. [CrossRef]
20. Ahmadalipour, A.; Rana, A.; Moradkhani, H.; Sharma, A. Multicriteria evaluation of CMIP5 GCMs for climate change impact analysis. *Theor. Appl. Climatol.* **2017**, *128*, 71–87. [CrossRef]
21. Su, F.; Duan, X.; Chen, D.; Hao, Z.; Cuo, L. Evaluation of the global climate models in the CMIP5 over the Tibetan Plateau. *J. Clim.* **2013**, *26*, 3187–3208. [CrossRef]
22. O'Neill, B.C.; Tebaldi, C.; Van Vuuren, D.P.; Eyring, V.; Friedlingstein, P.; Hurtt, G.; Knutti, R.; Kriegler, E.; Lamarque, J.-F.; Lowe, J.; et al. The Scenario Model Intercomparison Project (ScenarioMIP) for CMIP6. *Geosci. Model Dev.* **2016**, *9*, 3461–3482. [CrossRef]
23. Eyring, V.; Flato, G.; Lamarque, J.-F.; Meehl, J.; Senior, C.; Stouffer, R.; Taylor, K. Status of the Coupled Model Intercomparison Project Phase 6 (CMIP6) and Goals of the Workshop. In Proceedings of the CMIP6 Analysis Workshop, Barcelona, Spain, 25 March 2019.
24. Gidden, M.J.; Riahi, K.; Smith, S.J.; Fujimori, S.; Luderer, G.; Kriegler, E.; Van Vuuren, D.P.; Berg, M.V.D.; Feng, L.; Klein, D.; et al. Global emissions pathways under different socioeconomic scenarios for use in CMIP6: A dataset of harmonized emissions trajectories through the end of the century. *Geosci. Model Dev.* **2019**, *12*, 1443–1475. [CrossRef]
25. van Vuuren, D.; Edmonds, J.; O'Neill, B.; Moss, R.; Weyant, J.; Riahi, K. SSP/RCP-Based Scenarios for CMIP6. Available online: https://www.wcrp-climate.org/images/modelling/WGCM/WGCM17/8a_vanvuuren.pdf (accessed on 24 July 2021).
26. Almazroui, M.; Saeed, F.; Saeed, S.; Islam, M.N.; Ismail, M.; Klutse, N.A.B.; Siddiqui, M.H. Projected Change in Temperature and Precipitation Over Africa from CMIP6. *Earth Syst. Environ.* **2020**, *4*, 455–475. [CrossRef]
27. Kawai, H.; Yukimoto, S.; Koshiro, T.; Oshima, N.; Tanaka, T.; Yoshimura, H.; Nagasawa, R. Significant improvement of cloud representation in the global climate model MRI-ESM2. *Geosci. Model Dev.* **2019**, *12*, 2875–2897. [CrossRef]
28. Nawaz, N.R.; Bellerby, T.; Sayed, M.; Elshamy, M. Blue Nile Runoff Sensitivity to Climate Change. *Open Hydrol.* **2010**, *4*, 137–151. [CrossRef]
29. Zerfu, S.A.; Moges, T. Low flow analysis and regionalization of the Blue Nile River basin. Master Thesis, Arbaminch University, Arbaminch, Ethiopia, 2009.
30. Tabari, H.; Taye, M.T.; Willems, P. Water availability change in central Belgium for the late 21st century. *Glob. Planet. Chang.* **2015**, *131*, 115–123. [CrossRef]
31. McCartney, M.P.; Girma, M.M. Evaluating the downstream implications of planned water resource development in the Ethiopian portion of the Blue Nile River. *Water Int.* **2012**, *37*, 362–379. [CrossRef]
32. Kim, U.; Kaluarachchi, J.J. Climate Change Impacts on Water Resources in the Upper Blue Nile River Basin, Ethiopia. *JAWRA J. Am. Water Resour. Assoc.* **2009**, *45*, 1361–1378. [CrossRef]
33. Tafesse, T. The Hydropolitical Assessment of the Nile Question: An Ethiopian Perspective. *Water Int.* **2001**, *26*, 1–11. [CrossRef]
34. Kim, U.; Kaluarachchi, J.J. Application of parameter estimation and regionalization methodologies to ungauged basins of the Upper Blue Nile River Basin, Ethiopia. *J. Hydrol.* **2008**, *362*, 39–56. [CrossRef]
35. Harris, I.R.; Jones, P.; Osborn, T.; Lister, D. Updated high-resolution grids of monthly climatic observations—The CRU TS3.10 Dataset. *Int. J. Clim.* **2013**, *34*, 623–642. [CrossRef]
36. Rudolf, B.; Beck, C.; Grieser, J.; Schneider, U. Global Precipitation Analysis Products of the GPCC. 2005. Available online: https://www.researchgate.net/publication/266219519_Global_Precipitation_Analysis_Products_of_the_GPCC (accessed on 24 July 2021).
37. Hersbach, H.; Bell, B.; Berrisford, P.; Hirahara, S.; Horanyi, A.; Muñoz-Sabater, J.; Nicolas, J.; Peubey, C.; Radu, R.; Schepers, D.; et al. The ERA5 global reanalysis. *Q. J. R. Meteorol. Soc.* **2020**, *146*, 1999–2049. [CrossRef]
38. Saha, S.; Moorthi, S.; Wu, X.; Wang, J.; Nadiga, S.; Tripp, P.; Behringer, D.; Hou, Y.-T.; Chuang, H.-Y.; Iredell, M.; et al. The NCEP Climate Forecast System Version 2. *J. Clim.* **2014**, *27*, 2185–2208. [CrossRef]

39. Randles, C.; Da Silva, A.M.; Buchard, V.; Colarco, P.R.; Darmenov, A.; Govindaraju, R.; Smirnov, A.; Holben, B.; Ferrare, R.; Hair, J.; et al. The MERRA-2 Aerosol Reanalysis, 1980 Onward. Part I: System Description and Data Assimilation Evaluation. *J. Clim.* **2017**, *30*, 6823–6850. [CrossRef]
40. Wu, T.; Lu, Y.; Fang, Y.; Xin, X.; Li, L.; Li, W.; Jie, W.; Zhang, J.; Liu, Y.; Zhang, L.; et al. The Beijing Climate Center Climate System Model (BCC-CSM): The main progress from CMIP5 to CMIP6. *Geosci. Model Dev.* **2019**, *12*, 1573–1600. [CrossRef]
41. Swart, N.C.; Cole, J.N.S.; Kharin, V.V.; Lazare, M.; Scinocca, J.F.; Gillett, N.P.; Anstey, J.; Arora, V.; Christian, J.R.; Hanna, S.; et al. The Canadian Earth System Model version 5 (CanESM5.0.3). *Geosci. Model Dev.* **2019**, *12*, 4823–4873. [CrossRef]
42. Lauritzen, P.H.; Nair, R.D.; Herrington, A.R.; Callaghan, P.; Goldhaber, S.; Dennis, J.M.; Bacmeister, J.T.; Eaton, B.E.; Zarzycki, C.M.; Taylor, M.A.; et al. NCAR Release of CAM-SE in CESM2.0: A Reformulation of the Spectral Element Dynamical Core in Dry-Mass Vertical Coordinates with Comprehensive Treatment of Condensates and Energy. *J. Adv. Model. Earth Syst.* **2018**, *10*, 1537–1570. [CrossRef]
43. Liu, S.-M.; Chen, Y.-H.; Rao, J.; Cao, C.; Li, S.-Y.; Ma, M.-H.; Wang, Y.-B. Parallel Comparison of Major Sudden Stratospheric Warming Events in CESM1-WACCM and CESM2-WACCM. *Atmosphere* **2019**, *10*, 679. [CrossRef]
44. Wang, Y.; Yu, Z.; Lin, P.; Liu, H.; Jin, J.; Li, L.; Tang, Y.; Dong, L.; Chen, K.; Li, Y.; et al. FGOALS-g3 model datasets for CMIP6 flux-anomaly-forced model intercomparison project. *Adv. Atmos. Sci.* **2020**, *37*, 1093–1101. [CrossRef]
45. Fenta Mekonnen, D.; Disse, M. Analyzing the future climate change of Upper Blue Nile River basin using statistical downscaling techniques. *Hydrol. Earth Syst. Sci.* **2018**, *22*, 2391–2408. [CrossRef]
46. Tatebe, H.; Ogura, T.; Nitta, T.; Komuro, Y.; Ogochi, K.; Takemura, T.; Kimoto, M. Description and basic evaluation of simulated mean state, internal variability, and climate sensitivity in MIROC6. *Geosci. Model Dev.* **2019**, *12*. [CrossRef]
47. Sellar, A.A.; Walton, J.; Jones, C.G.; Wood, R.; Abraham, N.L.; Andrejczuk, M.; Andrews, M.B.; Andrews, T.; Archibald, A.T.; De Mora, L.; et al. Implementation of U.K. Earth System Models for CMIP6. *J. Adv. Model. Earth Syst.* **2020**, *12*. [CrossRef]
48. Stern, R.; Rijks, D.; Dale, I.; Knock, J. *INSTAT Climatic Guide*; Statistical Services Centre, University of Reading: Reading, UK, 2006; pp. 247–281.
49. Piani, C.; Haerter, J.O.; Coppola, E. Statistical bias correction for daily precipitation in regional climate models over Europe. *Theor. Appl. Clim.* **2009**, *99*, 187–192. [CrossRef]
50. Ringard, J.; Seyler, F.; Linguet, L. A Quantile Mapping Bias Correction Method Based on Hydroclimatic Classification of the Guiana Shield. *Sensors* **2017**, *17*, 1413. [CrossRef] [PubMed]
51. Gudmundsson, L.; Bremnes, J.B.; Haugen, J.E.; Engenskaugen, T. Technical Note: Downscaling RCM precipitation to the station scale using statistical transformations—A comparison of methods. *Hydrol. Earth Syst. Sci.* **2012**, *16*, 3383–3390. [CrossRef]
52. Gudmundsson, L. Statistical Transformations for Post-Processing Climate Model Output. 2016. Available online: https://hess.copernicus.org/articles/16/3383/2012/ (accessed on 24 July 2021).
53. Taylor, K.E. Summarizing multiple aspects of model performance in a single diagram. *J. Geophys. Res.* **2001**, *106*, 7183–7192. [CrossRef]
54. Mann, H.B. Nonparametric Tests against Trend. *Econometrica* **1945**, *13*, 245–259. [CrossRef]
55. Khambhammettu, P. *Mann-Kendall analysis for the Fort Ord Site*; Hydrogeol. Inc.: Austin, TX, USA, 2005; pp. 1–7.
56. Yue, S.; Pilon, P.; Cavadias, G. Power of the Mann–Kendall and Spearman's rho tests for detecting monotonic trends in hydrological series. *J. Hydrol.* **2002**, *259*, 254–271. [CrossRef]
57. Egeru, A.; Barasa, B.; Nampijja, J.; Siya, A.; Makooma, M.T.; Majaliwa, M.G.J. Past, present and future climate trends under varied representative concentration pathways for a sub-humid region in Uganda. *Climate* **2019**, *7*, 35. [CrossRef]
58. Zambrano-Bigiarini, M.; Nauditt, A.; Birkel, C.; Verbist, K.; Ribbe, L. Temporal and spatial evaluation of satellite-based rainfall estimates across the complex topographical and climatic gradients of Chile. *Hydrol. Earth Syst. Sci.* **2017**, *21*, 1295–1320. [CrossRef]
59. Beyene, T.; Lettenmaier, D.P.; Kabat, P. Hydrologic impacts of climate change on the Nile River Basin: Implications of the 2007 IPCC scenarios. *Clim. Chang.* **2009**, *100*, 433–461. [CrossRef]
60. Mengistu, D.; Bewket, W.; Dosio, A.; Panitz, H.-J. Climate change impacts on water resources in the Upper Blue Nile (Abay) River Basin, Ethiopia. *J. Hydrol.* **2021**, *592*, 125614. [CrossRef]
61. Themeßl, M.J.; Gobiet, A.; Heinrich, G. Empirical-statistical downscaling and error correction of regional climate models and its impact on the climate change signal. *Clim. Chang.* **2011**, *112*, 449–468. [CrossRef]
62. Dosio, A.; Jones, R.G.; Jack, C.; Lennard, C.; Nikulin, G.; Hewitson, B. What can we know about future precipitation in Africa? Robustness, significance and added value of projections from a large ensemble of regional climate models. *Clim. Dyn.* **2019**, *53*, 5833–5858. [CrossRef]
63. Aich, V.; Liersch, S.; Vetter, T.; Huang, S.; Tecklenburg, J.; Hoffmann, P.; Koch, H.E.; Fournet, S.; Krysanova, V.; Müller, E.N.; et al. Comparing impacts of climate change on streamflow in four large African river basins. *Hydrol. Earth Syst. Sci.* **2014**, *18*, 1305–1321. [CrossRef]
64. Legesse, S.A. The outlook of Ethiopian long rain season from the global circulation model. *Environ. Syst. Res.* **2016**, *5*, 577. [CrossRef]
65. Haile, A.T.; Akawka, A.L.; Berhanu, B.; Rientjes, T. Changes in water availability in the Upper Blue Nile basin under the representative concentration pathways scenario. *Hydrol. Sci. J.* **2017**, *62*, 2139–2149. [CrossRef]
66. Girma, M.M. Potential Impact of Climate and Land Use Changes on the Water Resources of the Upper Blue Nile Basin. Master Thesis, Freie University of Berlin, Berlin, Germany, 2013; pp. 1–103.

67. Cherie, N.Z. Downscaling and Modeling the Effects of Climate Change on Hydrology and Water Resources in the Upper Blue Nile River Basin, Ethiopia. Ph.D. Thesis, University of Kassel, Kassel, Germany, 2013; pp. 1–329.
68. Wagena, M.B.; Sommerlot, A.; Abiy, A.Z.; Collick, A.S.; Langan, S.; Fuka, D.R.; Easton, Z.M. Climate change in the Blue Nile Basin Ethiopia: Implications for water resources and sediment transport. *Clim. Chang.* **2016**, *139*, 229–243. [CrossRef]
69. Getachew, B.; Manjunatha, B.; Bhat, H.G. Modeling projected impacts of climate and land use/land cover changes on hydrological responses in the Lake Tana Basin, upper Blue Nile River Basin, Ethiopia. *J. Hydrol.* **2021**, *595*, 125974. [CrossRef]
70. Dosio, A.; Turner, A.G.; Tamoffo, A.T.; Sylla, M.B.; Lennard, C.; Jones, R.G.; Terray, L.; Nikulin, G.; Hewitson, B. A tale of two futures: Contrasting scenarios of future precipitation for West Africa from an ensemble of regional climate models. *Environ. Res. Lett.* **2020**, *15*, 064007. [CrossRef]
71. Dosio, A.; Panitz, H.-J.; Schubert-Frisius, M.; Lüthi, D. Dynamical downscaling of CMIP5 global circulation models over CORDEX-Africa with COSMO-CLM: Evaluation over the present climate and analysis of the added value. *Clim. Dyn.* **2014**, *44*, 2637–2661. [CrossRef]
72. Yimer, G.; Jonoski, A.; Van Griensven, A. Hydrological response of a catchment to climate change, case study on Upper Beles Sub-Basin, Upper Blue Nile, Ethiopia. *Nile Basin Water Eng. Sci. Mag.* **2009**, *2*, 49–59.
73. Cherinet, A.A.; Yan, D.; Wang, H.; Song, X.; Qin, T.; Kassa, M.T.; Girma, A.; Dorjsuren, B.; Gedefaw, M.; Wang, H.; et al. Climate trends of temperature, precipitation and river discharge in the Abbay river basin in Ethiopia. *J. Water Resour. Prot.* **2019**, *11*, 1292. [CrossRef]
74. Iturbide, M.; Gutiérrez, J.M.; Alves, L.M.; Bedia, J.; Cerezo-Mota, R.; Cimadevilla, E.; Cofiño, A.S.; Di Luca, A.; Faria, S.H.; Gorodetskaya, I.V.; et al. An update of IPCC climate reference regions for subcontinental analysis of climate model data: Definition and aggregated datasets. *Earth Syst. Sci. Data* **2020**, *12*, 2959–2970. [CrossRef]